Effect of pointing errors on the performance of hybrid FSO/RF networks

Sharma, Shubha; Madhukumar, A. S.; Swaminathan, R.

2019

Sharma, S., Madhukumar, A. S., & Swaminathan, R. (2019). Effect of pointing errors on the performance of hybrid FSO/RF networks. IEEE Access, 7, 131418-131434. doi:10.1109/ACCESS.2019.2940630

https://hdl.handle.net/10356/144832

https://doi.org/10.1109/ACCESS.2019.2940630

IEEE Access
Multidisciplinary | Rapid Review | Open Access Journal

Received August 12, 2019, accepted August 24, 2019, date of publication September 10, 2019,
date of current version September 25, 2019.

Digital Object Identifier 10.1109/ACCESS.2019.2940630

Effect of Pointing Errors on the Performance of Hybrid FSO/RF Networks

SHUBHA SHARMA[1], (Student Member, IEEE),
A. S. MADHUKUMAR[1], (Senior Member, IEEE),
AND R. SWAMINATHAN[2], (Member, IEEE)
[1]School of Computer Science and Engineering, Nanyang Technological University, Singapore 639798
[2]Discipline of Electrical Engineering, IIT Indore, Indore 453552, India

Corresponding author: Shubha Sharma (shubha002@e.ntu.edu.sg)

This work was supported by the Singapore Ministry of Education Academic Research Fund Tier 1 Grant.

ABSTRACT The performance of a free space optics (FSO) transmission suffers from the atmospheric turbulence and the attenuation in foggy environment. By employing relay nodes, the error rate and the coverage area of the FSO communication system can be significantly improved. However, the pointing errors, generated because of the building sway, have the potential to eradicate the benefits of the relay-based FSO communication system. The effect of pointing errors in the presence of Gamma Gamma atmospheric fading together with path loss attenuation is considered in this paper. To counteract the adverse affects of the FSO link, a reliable millimeter-wave radio frequency (MMW RF) link is used as a backup. In this context, this paper proposes a cooperative decode-and-forward (DF)-relaying-based hybrid FSO/RF system with maximal-ratio-combining (MRC) at the destination. The system consists of FSO and RF sub-systems, where FSO sub-system has the priority to transmit and RF sub-system serves as a back up when the FSO sub-system is in outage. The exact and asymptotic outage probability and average symbol error rate (SER) expressions for the proposed system are derived in closed-form and the diversity order is determined. The effect of pointing errors on the system performance is analyzed extensively. The optimum values of transmit beam waist and radius of receiver aperture are determined. The theoretical results, which are validated by Monte-Carlo simulations, show that the proposed cooperative hybrid FSO/RF system drastically improves the system performance compared to single hop (SH) hybrid FSO/RF and cooperative FSO systems especially for large pointing errors scenario.

INDEX TERMS Hybrid FSO/RF systems, decode-and-forward relaying, pointing errors, gamma-gamma distribution, maximal-ratio-combining.

I. INTRODUCTION

Free space optics (FSO) communication has attracted significant importance to provide gigabit capacity links owing to its unique features: cheap installation cost with faster deployment, unlicensed spectrum, narrow laser beam enabling numerous FSO links. However, despite of many advantages, FSO supports high data rate only for short-range transmission and its performance is limited by the adverse effects of the atmospheric turbulence induced fading, attenuation due to fog, and pointing errors [1]. Therefore, to improve the performance of FSO links, it is wise to backup with reliable millimeter-wave radio frequency (MMW RF) links [1], [2]. Meanwhile, FSO and MMW RF channels exhibit complementary characteristics to fog and rain. Therefore, these complementary characteristics pave the way for hybrid FSO/MMW RF communication, which provides reliable high data rate transmission [2].

Mixed RF-FSO systems, where FSO is used as a last mile access link, use the concept of relaying technique to enhance the coverage and to counteract atmospheric turbulence induced fading and attenuation due to fog, thereby achieving some improvement in the system performance. In [3]–[8], a detailed performance analysis is presented for a dual-hop mixed RF-FSO communication system. The RF link is Nakagami-*m* distributed and the FSO link is

The associate editor coordinating the review of this manuscript and approving it for publication was Min Li.

characterized by Gamma-Gamma turbulence in [3]–[5] and effect of pointing errors is included in [6]–[8]. Besides in [9], the relay-destination link is a parallel FSO/RF link. It is worth noticing that the mentioned approaches analyze the performance of DH mixed RF-FSO systems without the presence of direct source-destination link except [10] which considers an RF source-destination link. Therefore, it is appropriate to assume that in a mixed RF-FSO system, FSO link transmission is confined as the last mile transmission.

Hybrid FSO/RF systems, where the RF link is used in parallel with the FSO link, improve the performance and reliability, as the RF link is less susceptible to atmospheric turbulence and attenuation due to fog. In [11], RF link is used in parallel with the FSO link and the diversity combining is employed at the receiver to combine the data from both the links. Diversity combining is applied to the signals with same data rate, therefore the data rate of the FSO transmission is reduced to that of the RF transmission. The schemes in [12]–[14], support higher data rates by assigning higher priority for FSO links and with the help of a single-bit feedback signal, RF transmission is activated when signal-to-noise ratio (SNR) of the FSO link is poor. It is to be noted that the hybrid schemes in [11]–[14] are confined to a single-hop (SH) system. To ensure coverage and reliability, we have analyzed the performance of DF-relaying-based dual-hop (DH) hybrid FSO/RF system considering selection combining (SC) and maximal-ratio-combining (MRC) in [15] and [16], respectively. However, the above mentioned hybrid schemes are restricted to atmospheric turbulence induced fading for FSO link and the effect of pointing errors has been ignored. For a more realistic and practical scenario, the effect of pointing errors must be considered [17].

Pointing errors is an adverse effect which greatly impacts the performance of FSO links mainly due to misalignment between transmit and receive apertures because of wind, earthquake and thermal expansion. To alleviate the issue of misalignment, optical beams with large radius can be used but at the price of reduced power levels or increased error rate at the receiver and less link security. Therefore, beam width optimization is important to achieve minimum error rate and geometric signal losses. Transmit apertures designed for FSO channels need to have accurate control of their beam widths, as significant gains can be made with the proper selection of beam width. Another method is to use MMW RF link as a backup, as they are less susceptible to pointing errors. However, the transmission data rate is compromised.

Gamma-Gamma atmospheric turbulence induced fading has gained wide acceptance in the current literature [2]–[20]. The most realistic modeling of FSO transmission links is based on Gamma-Gamma distribution due to its close similarity with experimental results for a wide range of atmospheric turbulence conditions [21]. The Gamma-Gamma distribution is represented in terms of the modified Bessel function of the second kind, and therefore, it is very challenging to analyze the performance of a DF-relaying-based hybrid FSO/RF system under the Gamma Gamma fading with pointing errors and path loss attenuation. In [20], by using a power series representation of the modified Bessel function, approximate error rate of the binary modulation is derived for equal gain combining (EGC) and MRC over the Gamma Gamma fading. In [19], the power series representation of Gamma Gamma fading with pointing errors is used to analyze the performance of FSO MIMO links.

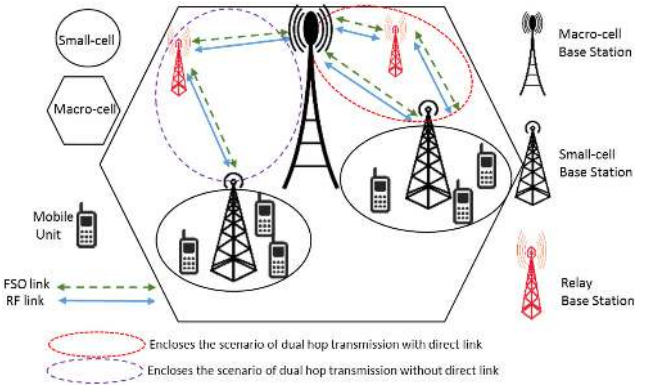

FIGURE 1. Architecture of hybrid FSO/RF system.

In this context, the present paper proposes a DF-relaying-based hybrid FSO/RF system using MRC at the destination, as shown in Fig. 1. We use DF-relaying protocol, where the transmission is conditioned on successful decoding at the relay [21]. It comprises of FSO and RF sub-systems, where RF sub-system serves as a backup. The FSO sub-system has higher priority to initiate and continue the transmission until the received SNR at the optical receiver fall below the threshold, γ_{th}. When the received SNR is less than γ_{th}, the FSO sub-system gets deactivated and the backup RF sub-system gets activated. In contrast to [3]–[10], the present work does not restrict FSO transmission to last mile access alone. The main objective of this work is to minimize the effect of turbulence, pointing errors, and attenuation using backup RF links and improve the performance of the overall system. In this context we highlight the motivations and contributions of our work as follows:

A. MOTIVATIONS

- To the best of our knowledge, the performance parameters in the presence of atmospheric turbulence, pointing errors, and path loss attenuation have been derived only for relay-based FSO system and not for hybrid FSO/RF system.
- The performance analysis of DF-relaying-based hybrid FSO/RF system has been restricted to the atmospheric turbulence induced fading for FSO link in our prior work [16]. Therefore, it is essential to investigate the importance of hybrid FSO/RF system in counteracting the effects of atmospheric turbulence, pointing errors, and path loss attenuation.
- To minimize the effect of pointing errors, transmit optical beam with large waist (or radius) can be used.

However, optical beams with large waist reduce link security and power levels at the receiver that results in performance degradation. . Therefore, the optimization of the transmit beam waist w_0 as well as radius of the receiver aperture a_j is important to achieve minimum error rate and minimum geometric signal losses. Another method to reduce the effect of pointing errors is to use RF links as a backup, since they are less susceptible to pointing errors. As per author's knowledge, the optimum values of w_0 and a_j and the usage of RF links as a backup to counteract pointing errors have never been presented in any of the prior works.

- The closed-form representation of probability density function (PDF) of the Gamma-Gamma distribution with pointing errors and path loss contains the Meijer-G function of a random variable. In prior works, the exact symbol error rate (SER) expressions solved using the PDF of FSO link (with pointing errors and path loss) were quiet complicated to comprehend. In case of DF-relaying-based hybrid FSO/RF system using MRC, it is mathematically intractable to derive the exact outage and symbol error rate (SER) expressions from the PDF containing multiple Meijer-G functions. Therefore, it is important to propose a simplified power series-based PDF for the FSO links to obtain the performance parameters of hybrid FSO/RF system.
- Simpler asymptotic expressions are also required to understand the system behavior and to derive the diversity order of the system in the presence of both pointing errors and atmospheric turbulence. In our prior work, asymptotic expressions were not derived for hybrid FSO/RF system considering both atmospheric turbulence induced fading and pointing errors.

B. CONTRIBUTIONS

- The performance of a novel DF-relaying-based hybrid FSO/RF system with MRC combining is investigated in the presence of atmospheric turbulence together with pointing errors for FSO links. The system also considers the path loss due to various weather conditions for both FSO and RF links. Note that MRC scheme is an optimum combining scheme, where output SNR is the weighted sum of SNRs of individual links.
- The analysis has been presented to calculate the optimum beam waist at the transmitter output w_0 and optimum radius of the receiver aperture a_j, which minimize the average SER. The values of w_0 and a_j are also calculated for different link distance L_j and weather conditions. Transmitter and receiver apertures designed for such FSO channels with different L_j and weather conditions need to have accurate control of w_0 and a_j, as significant gains can be made with the proper selection of beam waist at the transmitter and radius of receiver aperture.
- A simple power series-based representation is proposed for the PDF of Gamma-Gamma faded FSO links with pointing errors and path loss. This series representation becomes simple as it contains only the terms with exponent of the random variable.
- The performance analysis of the proposed system has been carried out by deriving exact closed-form and asymptotic expressions for outage probability and average SER. The average SER analysis is investigated by assuming sub-carrier intensity based M-ary phase-shift keying (MPSK) signaling for FSO sub-system and MPSK signaling for RF sub-system
- The asymptotic outage and SER expressions with lower computational complexity are derived in closed-form and the diversity order is determined. The proposed asymptotic analysis demonstrates that the diversity gain is dominated by pointing errors if they are aggressive than the atmospheric turbulence. Note that all the exact and asymptotic expressions are verified using Monte-Carlo simulation results.

The rest of the paper is organized as follows. The system and channel models of the proposed scheme are given in section II. Statistical characteristics of FSO and RF sub-systems are also discussed in section II. In section III and IV, outage and average SER analyses are given for the proposed scheme, respectively. The asymptotic outage and SER analyses are given in section V and VI, respectively. Section VII discusses the results of numerical analysis and the paper concludes at Section VIII.

II. SYSTEM AND CHANNEL MODEL

We consider a hybrid FSO/RF system comprising of a DF-relaying-based FSO and RF sub-systems. The sub-systems employ MRC to combine the data at the destination. A one-bit feedback message is required for the selection between FSO and RF sub-systems. The proposed system comprises of a source (S), relay (R), and destination (D). The atmospheric turbulence induced fading channels over FSO links S-D, S-R and R-D (I^{SD}, I^{SR}, and I^{RD}) are modeled using Gamma-Gamma distribution with pointing errors and path loss. There are few recently proposed models such as $\mathcal{M}$alaga Distribution [32] and Double generalized Gamma distribution [33], which are slightly more accurate than Gamma-Gamma distribution. In our forthcoming works, we may use the generalized fading models to analyze the system. The corresponding norm of the flat faded RF channel gains (h_{SD}, h_{SR}, and h_{RD}) are modeled using Nakagami-m distribution. We also consider path loss attenuation in different weather conditions for both FSO and MMW RF channels [16]. It is assumed that the channel gains of FSO and MMW RF links are mutually independent. The DF-relaying-based FSO and RF sub-systems works in two transmission phases, where S transmits the signal which is received by R and D in the first transmission phase. In the second phase, S remains silent and R transmits the decoded signal to D and MRC scheme is applied to retrieve the data from the received signals.

TABLE 1. Comprehensive list of notations used in the paper.

$\mathcal{K}_1^j = \frac{\xi_j^2}{2\Gamma(\alpha_j)\Gamma(\beta_j)}$	$C_1^j = \frac{csc(\pi(\alpha_j-\xi_j^2))csc(\pi(\beta_j-\xi_j^2))}{\Gamma(1)}$	$\kappa_j = \xi_j^2/(\xi_j^2+1)$	$\mathcal{N}_3^j = \frac{\xi_j^2}{2}, \frac{\xi_j^2+1}{2}, \frac{\alpha_j}{2}, \frac{\alpha_j+1}{2}, \frac{\beta_j}{2}, \frac{\beta_j+1}{2}$
$v_j \triangleq \frac{(\alpha_j\beta_j\kappa_j)^2}{16\bar{\gamma}_j^p}$	$C_2^j = \frac{csc(\pi(\xi_j^2-\alpha_j))csc(\pi(\beta_j-\alpha_j))}{\Gamma(\xi_j^2+1-\alpha_j)}$	$c \triangleq \frac{\xi_{SD}^2}{2}+1$	$\mathcal{N}_{4,n_1}^j = 1-n_1, \frac{\xi_j^2+1}{2}, \frac{\xi_j^2+2}{2}$
$w_j \triangleq \frac{m_j}{\bar{\gamma}_j^r}$	$C_3^j = \frac{csc(\pi(\xi_j^2-\beta_j))csc(\pi(\alpha_j-\beta_j))}{\Gamma(\xi_j^2+1-\beta_j)}$	$c_{n_1}^n \triangleq \Omega_{g,n}^{RD}+n_1$	$\mathcal{N}_{5,n_1}^j = \frac{\xi_j^2}{2}+n_1, \frac{\xi_j^2+1}{2}, \frac{\alpha_j}{2}, \frac{\alpha_j+1}{2}, \frac{\beta_j}{2}, \frac{\beta_j+1}{2}$
$\Omega_{1,n}^j = \frac{\xi_j^2+n}{2}$	$X_{1,n}^j \triangleq \frac{C_1^j(0)_n\left(v_j^p\right)^{\xi_j^2+n}}{n!\Gamma(n+1-\alpha_j+\xi_j^2)\Gamma(n+1-\beta_j+\xi_j^2)}$	$\mathcal{K}_2^j = \frac{\xi_j^2 2^{\alpha_j+\beta_j}}{8\pi\Gamma(\alpha_j)\Gamma(\beta_j)}$	$C_{n_2}^{k_1} \triangleq \frac{(-1)^{n_2+k_1} w_{SD}^{-k_1} w_{RD}^{m_{RD}+n_2}}{n_2!(m_{RD}+n_2)\Gamma(m_{SD})\Gamma(m_{RD})}\binom{m_{RD}+n_2}{k_1}$
$\Omega_{2,n}^j = \frac{\alpha_j+n}{2}$	$X_{2,n}^j \triangleq \frac{C_2^j(\alpha_j-\xi_j^2)_n\left(v_j^p\right)^{\alpha_j+n}}{n!\Gamma(n+1-\xi_j^2+\alpha_j)\Gamma(n+1-\beta_J+\alpha_j)}$	$C_{n_2,k_1}^{m,p_1} = (C_{n_2,k_1}^{m_{RD}}+p_1)$	$C_{n_2,k_1}^m \triangleq m_{RD}+n_2-k_1$
$\Omega_{3,n}^j = \frac{\beta_j+n}{2}$	$X_{3,n}^j \triangleq \frac{C_3^j(\beta_j-\xi_j^2)_n\left(v_j^p\right)^{\beta_j+n}}{n!\Gamma(n+1-\xi_j^2+\beta_j)\Gamma(n+1-\alpha_j+\beta_j)}$	$\mathcal{N}_1^j = \xi_j^2, \alpha_j, \beta_j$	$C_{k_1}^m \triangleq m_{SD}+k_1$
$\xi_j = \frac{w_{Leq_j}}{2\sigma_s^j}$	$\mathcal{K}_{n_3} = \frac{(-1)^{n_3} D^{2n_3+1}}{n_3!\,(2n_3+1)}$	$\mathcal{N}_2^j = 1, \frac{\xi_j^2+1}{2}, \frac{\xi_j^2+2}{2}$	$\mathcal{K}_{n_1} = \mathcal{K}_2^{SD}\mathcal{K}_2^{RD}\Gamma(\frac{\xi_{RD}^2}{2}+1)\frac{1}{n_1!}$

A. FSO CHANNEL MODEL

The channel gain I^j can be expressed as follows: $I^j = I_a^j I_l^j I_p^j$, where I_a^j, I_l^j and I_p^j are atmospheric turbulence, atmospheric path loss and pointing errors, respectively and $j \in \{SR,\ RD,\ SD\}$. The PDF of I_a^j is given as [2, Eq.(2)]

$$f_{I_a^j}(I_a) = \frac{2\left(\alpha_j\beta_j\right)^{\frac{\alpha_j+\beta_j}{2}}(I_a)^{\frac{\alpha_j+\beta_j}{2}-1}}{\Gamma(\alpha_j)\Gamma(\beta_j)} K_{\alpha_j-\beta_j}\left(2\sqrt{\alpha_j\beta_j I_a}\right), \quad (1)$$

where $K_v(\cdot)$ is the v_{th}-order modified Bessel function of second kind, α_j and β_j are the small scale and large scale parameters of the scattering environment of j^{th} link. Assuming spherical wave propagation, these parameters can be directly related to atmospheric conditions according to [18, Eq. (2,3)] as follows:

$$\alpha_j = \left[\exp\left(0.49\chi_j^2\left(1+0.56\chi_j^{12/5}\right)^{-7/6}\right)-1\right]^{-1},$$
$$\beta_j = \left[\exp\left(0.51\chi_j^2\left(1+0.69\chi_j^{12/5}\right)^{-5/6}\right)-1\right]^{-1}, \quad (2)$$

where $\chi_j^2 = 0.5C_n^2 k^{7/6} L_j^{11/6}$ is the Rytov variance, L_j is the j^{th} link distance in meters and C_n^2 is the refractive index structure parameter and is altitude-dependent. In general, C_n^2 varies from $10^{-13}(\mathrm{m}^{-\frac{2}{3}})$ (for strong turbulence) to $10^{-16}(\mathrm{m}^{-\frac{2}{3}})$ (for weak turbulence). The average gain or atmospheric path loss of the FSO link or the attenuation factor is determined by Beers-Lambert Law as [2]

$$I_l^j = exp(-\alpha_1 L_j), \quad (3)$$

where α_1 is a weather dependent attenuation coefficient (in 1/km). The attenuation due to geometric spread with pointing error r is expressed as [22]

$$I_p^j(r; L_j) \approx A_0 \exp\left(-\frac{2r^2}{w_{Leq_j}^2}\right), \quad (4)$$

where $A_0^j = \left|\mathrm{erf}(v_j)\right|^2$, $v_j = \frac{\sqrt{\pi}a_j}{\sqrt{2}w_{L_j}}$ and $w_{Leq_j}^2 = \frac{w_{L_j}^2\sqrt{\pi}erf(v_j)}{2v_j exp(-v_j^2)}$. A_0^j is the fraction of the collected power at $r=0$, $\mathrm{erf}(\cdot)$ is the error function, w_{Leq_j} is the equivalent beam waist. We can also relate w_{Leq_j} with Gaussian laser beam waist w_{L_j} at the distance L_j and receiver aperture radius a_j as [22]. The Gaussian beam waist w_{L_j} can be defined as [22]

$$w_{L_j} \approx w_0\sqrt{1+\Theta_{0j}(\lambda L_j/\pi w_0^2)^2},$$
$$\Theta_{0j} = 1+\frac{2w_0^2}{\rho_0^2(L_j)}, \quad \rho_0(L_j) = (0.55C_n^2 k^2 L_j)^{-3/5} \quad (5)$$

where w_0 is the beam waist at $L_j = 0$, $k = 2\pi/\lambda$ is the optical wave number, λ is the wavelength. Considering independent identical Gaussian distributions for the elevation and the horizontal displacement (sway), the radial displacement r at the receiver is modeled by a Rayleigh distribution

$$f_r(r) = \frac{r}{\sigma_s^2}\exp\left(\frac{r^2}{2\sigma_s^2}\right) \quad (6)$$

where σ_s^j is the jitter standard deviation at the receiver. Combining (5) and (6), the PDF of I_p^j can be expressed as

$$f_{I_p^j}(I_p) = \frac{\xi_j^2}{A_0^{\xi_j^2}}(I_p)^{\xi_j^2-1} \quad (7)$$

where ξ_j is the pointing error coefficient [22], which can be expressed in terms of jitter standard deviation σ_s^j and the equivalent beam waist w_{Leq_j} as follows:

$$\xi_j = \frac{w_{Leq_j}}{2\sigma_s^j}. \quad (8)$$

The PDF of I^j is given as [8, Eq.(13)]

$$f_{I^j}(I) = \frac{\xi_j^2\alpha_j\beta_j}{A_0^j I_l^j \Gamma(\alpha_j)\Gamma(\beta_j)} G_{1,3}^{3,0}\left(\frac{\alpha_j\beta_j}{A_0^j I_l^j} I \,\middle|\, \begin{matrix}\xi_j^2\\ \xi_j^2-1,\ \alpha_j-1,\ \beta_j-1\end{matrix}\right), \quad (9)$$

The instantaneous electrical SNR at the output of the FSO receiver is given by

$$\gamma_j^p = \frac{\left|I^j\right|^2 P_j^2 \eta_j^2}{\sigma_j^2}, \quad (10)$$

where P_j is the transmitted optical power and I^j is the FSO channel fading coefficient with $E[I^j] = 1$, where $E[.]$ is the

expectation operator. The σ_j^2 is the variance of additive white Gaussian noise with zero mean, η_j is the optical-to-electrical conversion coefficient of the j_{th} link. The average SNR of any given FSO link is given by

$$\bar{\gamma}_j^p = \frac{P_j^2 \eta_j^2}{\sigma_j^2} \kappa_j^2 (A_0^j)^2 I_l^2, \tag{11}$$

where $\kappa_j = \xi_j^2/(\xi_j^2+1)$. In Table 1, the list of constants that are used throughout the paper are defined. Using power transformation of random variables, the PDF of instantaneous SNR of FSO link is given by

$$f_{\gamma_j^p}(\gamma) = \mathcal{K}_1^j \gamma^{-1} G_{1,3}^{3,0}\left(\frac{\alpha_j\beta_j\kappa_j}{\sqrt{\bar{\gamma}_j^p}}\sqrt{\gamma}\,\middle|\,\begin{matrix}\xi_j^2+1\\ \mathcal{N}_1^j\end{matrix}\right), \tag{12}$$

where $\mathcal{K}_1^j$ and $\mathcal{N}_1^j$ are given in Table 1. Using (12) and utilizing [23, Eq.(07.34.21.0084.01)], the cumulative distribution function (CDF) of γ_j^p is

$$F_{\gamma_j^p}(\gamma) = 2\mathcal{K}_1^j G_{2,4}^{3,1}\left(\frac{\alpha_j\beta_j\kappa_j}{\sqrt{\bar{\gamma}_j^p}}\sqrt{\gamma}\,\middle|\,\begin{matrix}1, \xi_j^2+1\\ \mathcal{N}_1^j, 0\end{matrix}\right). \tag{13}$$

It is noticed from (12) that the PDF of the FSO channel with pointing errors and path loss contains Meijer-G function of γ. It is infeasible to derive the exact outage and average SER expressions for the proposed system with MRC, as it is required to deal with multiple such Meijer-G functions. Therefore, we need a simple power series representation of (12), which can render simplified analysis.

B. POWER SERIES REPRESENTATION

Using [24], the Meijer G function in (12) can be written in terms of simple hypergeometric functions and the PDF $f_{\gamma_j^p}(\gamma)$ is given by

$$\begin{aligned} f_{\gamma_j^p}(\gamma) = \mathcal{K}_1^j \frac{\pi^2}{\gamma}\Bigg[& C_1^j \left(v_j^p\sqrt{\gamma}\right)^{\xi^2} {}_1\tilde{\mathrm{F}}_2(0;\, 1-\alpha+\xi^2,\\ & 1-\beta+\xi^2;\, v_j^p\sqrt{\gamma})\\ & + C_2^j \left(v_j^p\sqrt{\gamma}\right)^{\alpha} {}_1\tilde{\mathrm{F}}_2\left(\alpha-\xi^2;\, 1-\xi^2+\alpha,\right.\\ & \left. 1-\beta+\alpha;\, v_j^p\sqrt{\gamma}\right)\\ & + C_3^j \left(v_j^p\sqrt{\gamma}\right)^{\beta} {}_1\tilde{\mathrm{F}}_2\left(\beta-\xi^2;\, 1-\xi^2+\beta,\right.\\ & \left. 1-\alpha+\beta;\, v_j^p\sqrt{\gamma}\right)\Bigg] \end{aligned} \tag{14}$$

where ${}_p\tilde{\mathrm{F}}_q\left(a_{1,\ldots,}a_p; b_{1,\ldots,}b_q; z\right)$ is a regularized generalized hypergeometric function [23, Eq.(07.32.02.0001.01)], C_1^j, C_2^j, and C_3^j are given in Table 1. The regularized generalized hypergeometric function is given by

$${}_p\tilde{\mathrm{F}}_q\left(a_1\ldots a_p; b_1,\ldots,b_q; z\right) = \sum_{n=0}^{\infty} \frac{\prod_{j=1}^{p}(a_j)_n z^n}{n!\prod_{j=1}^{q}\Gamma(n+b_j)}, \tag{15}$$

where $(a_1)_n$ is the Pochhammer symbol [23, Eq.(06.10.02. 0001.01)]. Finally, the PDF of instantaneous SNR of FSO link in terms of power series is given by

$$f_{\gamma_j^p}(\gamma) = \mathcal{K}_1^j \pi^2 \sum_{n=0}^{\infty}\sum_{g=1}^{3} X_{g,n}^j \gamma^{\Omega_{g,n}^j - 1}, \tag{16}$$

where $X_{g,n}^j$ and $\Omega_{g,n}^j$ are given in Table 1. It is to be noted that the series in (16) contains summation terms with only exponents of γ. Therefore, it is easy to calculate an integral containing the proposed series representation as compared to a Meijer G function-based representation in (12).

C. MMW RF CHANNEL MODELING

The instantaneous received SNR (γ_j^r) and average SNR ($\overline{\gamma}_j^r$) of any given MMW RF link can be expressed, respectively, as

$$\gamma_j^r = \overline{\gamma}_j^r \left|h_j\right|^2, \quad \overline{\gamma}_j^r = \frac{P_j^r g_j^r}{\sigma_{rj}^2} \tag{17}$$

where P_j^r is the transmitted power, h_j is the RF channel fading with $E[|h_j|^2] = 1$. The norm of the fading channel gain i.e. $|h_j|$ is modeled as Nakagami-m distribution, where m indicates the fading severity parameter and it represents a wide variety of realistic line-of-sight (LOS) (with high values for m [12], [14]–[16]) and non-LOS fading channels encountered in practice. The σ_{rj}^2 is the variance of additive white Gaussian noise with zero mean and g_j^r is the path loss of RF link, which is given by [2]

$$g_j^r[dB] = G_t + G_r - 20\log_{10}(4\pi L_j/\lambda_r) - (\alpha_{oxy} + \alpha_{rain})L_j, \tag{18}$$

where L_j is the j^{th} link distance in meters, G_t and G_r denote the transmit and receive antenna gains, respectively, λ_r is the wavelength of the RF system, and α_{oxy} and α_{rain} are the attenuation caused by oxygen absorption and rain, respectively. The noise variance in the RF link is given by σ_{rj}^2 [dBm] = $B + N_o + N_F$ [2], where B is the RF bandwidth (in dBMHz), N_o is the noise power spectral density (in dBm/MHz), and N_F is the noise figure of the receiver. The PDF of γ_j^r, which follows Gamma distribution, is given by

$$f_{\gamma_j^r}(\gamma) = w_j^m \frac{\gamma^{m_j-1}}{\Gamma(m_j)} e^{-w_j\gamma}. \tag{19}$$

where w_j is given in Table 1. By using [25, Eq. (3.351.1)], the CDF of γ_j^r can be expressed as

$$F_{\gamma_j^r}(\gamma) = \frac{1}{\Gamma(m_j)}\gamma\left(m_j, w_j\gamma\right), \tag{20}$$

where $\gamma(\cdot,\cdot)$ is the lower incomplete gamma function [25, Eq. (8.350.1)].

III. OUTAGE ANALYSIS

In the proposed hybrid FSO/RF system, FSO sub-system initiates and continues to transmit until the received SNR is above the threshold SNR γ_{th}. If the FSO SNR goes below

γ_{th}, the FSO sub-system gets deactivated and the backup RF sub-system gets activated. The system is declared to be in outage, if the received SNRs of both FSO and MMW RF sub-systems are below γ_{th}. A one-bit feedback signal is used to activate the FSO or RF sub-system [26]. The feedback signaling is described as follows: According to the one bit feedback received from D, the following vectors are chosen i.e. either $\mathrm{v_f} = [a, 1-a]^{\mathrm{T}}$ for FSO or $\mathrm{v}_r = [1-a, a]^{\mathrm{T}}$ for RF transmission. It is assumed that there is no error in feedback, then the best strategy is to use $\mathrm{v_f}$ if $\gamma^p_{MRC} > \gamma_{th}$ and $\mathrm{v_r}$ if $\gamma^p_{MRC} < \gamma_{th}$, where $a = 1$ and γ^p_{MRC} is the instantaneous SNR of FSO sub-system after MRC [26]. The expression for outage probability is given by

$$P^p_{MRC} = F_{\gamma^p_{MRC}}(\gamma_{th}) F_{\gamma^r_{MRC}}(\gamma_{th}), \tag{21}$$

where $F_{\gamma^p_{MRC}}(\gamma_{th})$ and $F_{\gamma^r_{MRC}}(\gamma_{th})$ are the CDFs of the instantaneous SNRs of FSO and MMW RF links, respectively. The output SNR at D, conditioned on the successful decoding at R, is given by $\gamma^T_C = \gamma^T_{SD} + \gamma^T_{RD}$, where γ^T_{SD} and γ^T_{RD} represent the instantaneous SNRs of S–D and R–D links, respectively, and $T \in \{p,\ r\}$. Since γ^T_{SD} and γ^T_{RD} are independent random variables, the CDF of γ^T_C is given by

$$F_{\gamma^T_C}(\gamma) = \int_0^{\gamma} \int_0^{\gamma-\gamma^s} f_{\gamma^T_{RD}}(\gamma^k) f_{\gamma^T_{SD}}(\gamma^s) d\gamma^k d\gamma^s. \tag{22}$$

On the other hand, if R fails to decode in first transmission phase, it will remain silent in the second transmission phase. In this case, it is still possible for D to receive and decode the data through the direct S-D link. The CDF of γ^T_{MRC} in case of either FSO or RF transmission can be written as

$$F_{\gamma^T_{MRC}}(\gamma) = F_{\gamma^T_C}(\gamma)\left(1 - F_{\gamma^T_{SR}}(\gamma)\right) + F_{\gamma^T_{SR}}(\gamma) F_{\gamma^T_{SD}}(\gamma). \tag{23}$$

In case of FSO transmission, the inner integral in (22) is solved using [27, Eq. (2.24.2.2)]. The resultant expression is further simplified using [27, Eq.(6.11.1.1)]. Finally, the integral is solved using [27, Eq. (2.24.2.2)] to get the exact expression as

$$F_{\gamma^p_C}(\gamma) = \sum_{n_1=0}^{\infty} \mathcal{K}_{n_1} G^{6,1}_{3,7}\left(v_{RD}\gamma \middle| \begin{matrix} \mathcal{N}^{RD}_2 \\ \mathcal{N}^{RD}_{5,n_1}, 0 \end{matrix}\right) \times G^{6,1}_{3,7}\left(v_{SD}\gamma \middle| \begin{matrix} \mathcal{N}^{SD}_{4,n_1} \\ \mathcal{N}^{SD}_3, -(\frac{\xi^2_{RD}}{2} + n_1) \end{matrix}\right), \tag{24}$$

where $\mathcal{K}_{n_1}$, $\mathcal{N}^j_2$, $\mathcal{N}^j_3$, $\mathcal{N}^j_{4,n_1}$, and $\mathcal{N}^j_{5,n_1}$ are given in Table 1. In case of RF transmission, we solve (22) as in [28] to get the exact expression as

$$F_{\gamma^r_C}(\gamma) = \sum_{n_2=0}^{\infty} \sum_{k_1=0}^{m_{RD}+n_2} C^{k_1}_{n_2} \gamma^{C^m_{n_2,k_1}} \gamma\left(C^m_{k_1}, w_{SD}\gamma\right), \tag{25}$$

where $C^{k_1}_{n_2}$, $C^m_{n_2,k_1}$ and $C^m_{k_1}$ are given in Table 1. By substituting (13) and (24) into (23), we obtain $F_{\gamma^p_{MRC}}(\gamma_{th})$ and by substituting (20) and (25) into (23), we obtain $F_{\gamma^r_{MRC}}(\gamma_{th})$. By substituting $F_{\gamma^p_{MRC}}(\gamma_{th})$ and $F_{\gamma^r_{MRC}}(\gamma_{th})$ into (21), the outage probability of the proposed system is obtained.

The PDF of γ^r_C, obtained by differentiating (25) with respect to γ using [25, Eq.(8.352.6)], is given by (26), as shown at the bottom of this page. In order to obtain $f_{\gamma^p_C}(\gamma)$, we recalculate $F_{\gamma^p_C}(\gamma)$ and the inner integral in (22) is solved using [27, Eq. (2.24.2.2)]. The resultant expression is further simplified using [27, Eq.(6.11.1.1)]. Finally, the remaining integral is solved by substituting (16) and using [29, Eq.(3.191)] to get the exact expression as

$$F_{\gamma^p_C}(\gamma) = \mathcal{K}^{SD}_1 \mathcal{K}^{RD}_2 \pi^2 \sum_{n_1=0}^{\infty} \frac{1}{n_1!} G^{6,1}_{3,7}\left(v_{RD}\gamma \middle| \begin{matrix} \mathcal{N}^{RD}_2 \\ \mathcal{N}^{RD}_{5,n_1}, 0 \end{matrix}\right) \times \sum_{n=0}^{\infty} \sum_{g=1}^{3} X^{SD}_{g,n} \mathrm{B}(c, c^n_{n_1}) \gamma^{\Omega^{SD}_{g,n}}, \tag{28}$$

where $\mathcal{K}^j_1$, $\mathcal{K}^j_2$, v_j, $\mathcal{N}^j_2$, $\mathcal{N}^j_{5,n_1}$, $X^j_{g,n}$, c, $c^n_{n_1}$, and $\Omega^j_{g,n}$ are given in Table 1, $j \in \{SD, RD\}$, and $\mathrm{B}(\cdot,\cdot)$ is the beta function [25, Eq. (8.384.1)]. The PDF of γ^p_C, obtained by differentiating (28) with respect to γ, is given by (27), as shown at the bottom of this page.

A. ASYMPTOTIC OUTAGE ANALYSIS

At high electrical SNR of any given FSO link ($\bar{\gamma}^p_j$) and for a fixed value of average SNR of RF links, the asymptotic outage probability is given by

$$P^{p\infty}_{MRC} = F^{\infty}_{\gamma^p_{MRC}}(\gamma_{th}) F_{\gamma^r_{MRC}}(\gamma_{th}) \tag{29}$$

where $F_{\gamma^r_{MRC}}(\gamma_{th})$ is given by (23) and $F^{\infty}_{\gamma^p_{MRC}}(\gamma_{th})$ is given by

$$F^{\infty}_{\gamma^p_{MRC}}(\gamma_{th}) = F^{\infty}_{\gamma^p_C}(\gamma_{th})\left(1 - F^{\infty}_{\gamma^p_{SR}}(\gamma_{th})\right) + F^{\infty}_{\gamma^p_{SR}}(\gamma_{th}) F^{\infty}_{\gamma^p_{SD}}(\gamma_{th}). \tag{30}$$

$$f_{\gamma^r_C}(\gamma) = \sum_{n_2=0}^{\infty} \sum_{k_1=0}^{m_{RD}+n_2} C^{k_1}_{n_2} (C^m_{k_1} - 1)! \left[C^m_{n_2,k_1} \gamma^{C^m_{n_2,k_1}} - \sum_{p_1=0}^{C^m_{k_1}-1} \frac{w^{p_1}_{SD}}{p_1!} C^{m,p_1}_{n_2,k_1} \gamma^{C^{m,p_1}_{n_2,k_1}-1} e^{-w_{SD}\gamma} + \sum_{p_1=0}^{C^m_{k_1}-1} \frac{w^{p_1+1}_{SD}}{p_1!} \gamma^{C^{m,p_1}_{n_2,k_1}} e^{-w_{SD}\gamma} \right] \tag{26}$$

$$f_{\gamma^p_C}(\gamma) = \mathcal{K}^{SD}_1 \mathcal{K}^{RD}_2 \pi^2 \sum_{n_1=0}^{\infty} \sum_{n=0}^{\infty} \sum_{g=1}^{3} \frac{X^{SD}_{g,n} \mathrm{B}(\mathrm{c}, \mathrm{c}^{\mathrm{n}}_{\mathrm{n}_1})}{n_1!} \left[\gamma^{\Omega^{SD}_{gn}} G^{6,2}_{4,8}\left(v_{RD}\gamma \middle| \begin{matrix} 0, \mathcal{N}^{RD}_2 \\ \mathcal{N}^{RD}_{5,n_1}, 1, 0 \end{matrix}\right) + \Omega^{SD}_{g,n} \gamma^{\Omega^{SD}_{g,n}-1} G^{6,1}_{3,7}\left(v_{RD}\gamma \middle| \begin{matrix} \mathcal{N}^{RD}_2 \\ \mathcal{N}^{RD}_{5,n_1}, 0 \end{matrix}\right) \right] \tag{27}$$

Applying [23, Eq. (07.34.06.0044.01)] in (12), the CDF of the end-to-end SNR in the asymptotic regime is given as

$$F^{\infty}_{\gamma^p_j}(\gamma_{th}) \simeq 2\sum_{k=1}^{3} \mathcal{K}^j_1 \Lambda^j_{1,k} \left[\sqrt{\bar{\gamma}^p_j}\right]^{-\mathcal{N}^j_{1,k}}, \tag{31}$$

where $\Lambda^j_{1,k}$ is given in Table 2 and $j \in \{SD, SR\}$. The series in (31) can be further simplified by taking only the k^{th} term that is related to the minimum value of $\mathcal{N}_{1,k}$. Such an assumption is justified by the fact that at $\bar{\gamma}^p_j \to \infty$, we have term $\left[\frac{\alpha_j\beta_j\kappa_j}{\sqrt{\bar{\gamma}^p_j}}\sqrt{\gamma_{th}}\right]^{\mathcal{N}_{1,k}} \to 0$ for large $\mathcal{N}^j_{1,k}$ values. Accordingly, we get

$$F^{\infty}_{\gamma^p_j}(\gamma_{th}) \simeq 2\sum_{k=1}^{3} \mathcal{K}^j_1 \Lambda^j_{1,k} \left[\sqrt{\bar{\gamma}^p_j}\right]^{-v_j}, \tag{32}$$

where $v_j = \min\{\frac{\xi^2_j}{2}, \frac{\alpha_j}{2}, \frac{\beta_j}{2}\}$. By applying [23, Eq. (07.34.06.0040.01)] in (24), $F^{\infty}_{\gamma^p_C}(\gamma_{th})$ in the asymptotic regime is given as

$$F^{\infty}_{\gamma^p_C}(\gamma_{th}) \simeq \sum_{n_1=0}^{\infty}\sum_{k=1}^{6} \mathcal{K}_{n_1} \Lambda^{SD,n_1}_{2,k} \Lambda^{RD,n_1}_{3,k} \left[\bar{\gamma}^f_{SD}\right]^{-v_{SD}} \left[\bar{\gamma}^f_{RD}\right]^{-v_{RD}}, \tag{33}$$

where $\Lambda^{j,n_1}_{2,k}$ and $\Lambda^{j,n_1}_{3,k}$ are given in Table 2. By substituting (32) and (33) into (30), we obtain $F^{\infty}_{\gamma^p_{MRC}}(\gamma_{th})$. It is inferred from (30) that the diversity order depends on $F^{\infty}_{\gamma^p_C}(\gamma_{th})$ or $F^{\infty}_{\gamma^p_{SR}}(\gamma_{th})F^{\infty}_{\gamma^p_{SD}}(\gamma_{th})$. To calculate the diversity order, we assume $\bar{\gamma}^p_{SD} = \bar{\gamma}^p_{SR} = \bar{\gamma}^p_{RD} = \bar{\gamma}^p$. Therefore, the diversity order is given by $G_{op} = v_i + v_j$, where $i \in \{SR, RD\}$ and $j = SD$. It can be written as $G_{op} = \min\{\frac{\xi^2_i}{2}, \frac{\alpha_i}{2}, \frac{\beta_i}{2}\} + \min\{\frac{\xi^2_j}{2}\frac{\alpha_j}{2}, \frac{\beta_j}{2}\}$. Since $\alpha > \beta$ in (2), the diversity order can be simplified as $G_{op} = \min\{\frac{\xi^2_i}{2}, \frac{\beta_i}{2}\} + \min\{\frac{\xi^2_j}{2}, \frac{\beta_j}{2}\}$. If $\beta = \beta_j = \beta_i$ and $\xi = \xi_j = \xi_i$, then the diversity order is given by $G_{op} = \min\{\xi^2, \beta\}$.

IV. AVERAGE SER ANALYSIS

The average SER during non-outage period can be calculated in terms of the average SER of individual FSO and MMW RF links and is given by

$$\overline{SER}_{MRC} = \frac{B^p_{MRC}(\gamma_{th}) + F_{\gamma^p_{MRC}}(\gamma_{th})B^r_{MRC}(\gamma_{th})}{1 - P_{MRC}}, \tag{34}$$

where P_{MRC} is given by (21), $F_{\gamma^p_{MRC}}(\gamma_{th})$ is given by (23), $B^T_{MRC}(\gamma_{th})$, when $\gamma^T_{MRC} > \gamma_{th}$, is given by (35), as shown at the bottom of this page, where $p(e/\gamma)$ is the conditional SER for MPSK signaling conditioned on the instantaneous SNR of any given link γ and $f_{\gamma^T_{MRC}}(\gamma)$ is the PDF of both FSO and RF sub-systems. The detailed derivations of each term in (35) for $B^p_{MRC}(\gamma_{th})$ and $B^r_{MRC}(\gamma_{th})$ are given in Appendix A and B, respectively. The PDF $f_{\gamma^T_{MRC}}(\gamma)$ is obtained by differentiating (23) with respect to γ as

$$\begin{aligned} f_{\gamma^T_{MRC}}(\gamma) = {} & f_{\gamma^T_C}(\gamma) - f_{\gamma^T_C}(\gamma)F_{\gamma^T_{SR}}(\gamma) - F_{\gamma^T_C}(\gamma)f_{\gamma^T_{SR}}(\gamma) \\ & + f_{\gamma^T_{SR}}(\gamma)F_{\gamma^T_{SD}}(\gamma) + f_{\gamma^T_{SD}}(\gamma)F_{\gamma^T_{SR}}(\gamma). \end{aligned} \tag{36}$$

A. ASYMPTOTIC SER ANALYSIS

The asymptotic SER during non-outage period can be calculated in terms of the average SER of individual FSO and MMW RF links and is given by

$$\overline{SER}^{\infty}_{MRC} = \frac{B^{p\infty}_{MRC}(\gamma_{th}) + F^{\infty}_{\gamma^p_{MRC}}(\gamma_{th})B^r_{MRC}(\gamma_{th})}{1 - P^{\infty}_{MRC}}, \tag{37}$$

where P^{∞}_{MRC}, $F^{\infty}_{\gamma^p_{MRC}}(\gamma_{th})$, and $B^r_{MRC}(\gamma th)$ are given by (29), (30), and (35), respectively. Substituting $f_{\gamma^{p\infty}_{MRC}}(\gamma)$ (i.e. (36) in

TABLE 2. Notations used in asymptotic outage analysis.

$\Lambda^j_{1,k} = \frac{\prod_{q=1,q\neq k}^{3}\Gamma(\mathcal{N}^j_{1,q}-\mathcal{N}^j_{1,k})\Gamma(\mathcal{N}^j_{1,k})}{\Gamma(1+\xi^2_j-\mathcal{N}^j_{1,k})\Gamma(1+\mathcal{N}^j_{1,k})}\left(\alpha_j\beta_j\kappa_j\sqrt{\gamma_{th}}\right)^{\mathcal{N}^j_{1,k}}$
$\Lambda^{j,n_1}_{2,k} = \frac{\prod_{q=1,q\neq k}^{6}\Gamma(\mathcal{N}^j_{5,q}-\mathcal{N}^{j,n_1}_{5,k})\Gamma(\mathcal{N}^{j,n_1}_{5,k})}{\prod_{q=2}^{3}\Gamma(\mathcal{N}^j_{2,q}-\mathcal{N}^j_{2,k})\Gamma(1+\mathcal{N}^{j,n_1}_{5,k})}\left[\frac{(\alpha_j\beta_j\kappa_j)^2\gamma_{th}}{16}\right]^{\mathcal{N}^{j,n_1}_{5,k}}$
$\Lambda^{j,n_1}_{3,k} = \frac{\prod_{q=1,q\neq k}^{4}\Gamma(\mathcal{N}^j_{3,q}-\mathcal{N}^j_{3,k})\Gamma(n_1+\mathcal{N}^j_{3,k})}{\prod_{q=2}^{3}\Gamma(\mathcal{N}^{j,n_1}_{4,q}-\mathcal{N}^j_{3,k})\Gamma(1+n_1+\frac{\xi^2_j}{2}+\mathcal{N}^j_{3,k})}\left[\frac{(\alpha_j\beta_j\kappa_j)^2\gamma_{th}}{16}\right]^{\mathcal{N}^j_{3,k}}$

$$\begin{aligned} B^T_{MRC}(\gamma_{th}) = \int_{\gamma_{th}}^{\infty} p(e|\gamma)f_{\gamma^T_{MRC}}(\gamma)d\gamma &= \underbrace{\int_{\gamma_{th}}^{\infty} p(e|\gamma)f_{\gamma^T_C}(\gamma)d\gamma}_{B^T_C(\gamma_{th})} - \underbrace{\int_{\gamma_{th}}^{\infty} p(e|\gamma)f_{\gamma^T_C}(\gamma)F_{\gamma^T_{SR}}(\gamma)d\gamma}_{B^T_{C,SR}(\gamma_{th})} \\ & - \underbrace{\int_{\gamma_{th}}^{\infty} p(e|\gamma)f_{\gamma^T_{SR}}(\gamma)F_{\gamma^T_C}(\gamma)d\gamma}_{B^T_{SR,C}(\gamma_{th})} + \underbrace{\int_{\gamma_{th}}^{\infty} p(e|\gamma)f_{\gamma^T_{SR}}(\gamma)F_{\gamma^T_{SD}}(\gamma)d\gamma}_{B^T_{SR,SD}(\gamma_{th})} + \underbrace{\int_{\gamma_{th}}^{\infty} p(e|\gamma)f_{\gamma^T_{SD}}(\gamma)F_{\gamma^T_{SR}}(\gamma)d\gamma}_{B^T_{SD,SR}(\gamma_{th})} \end{aligned} \tag{35}$$

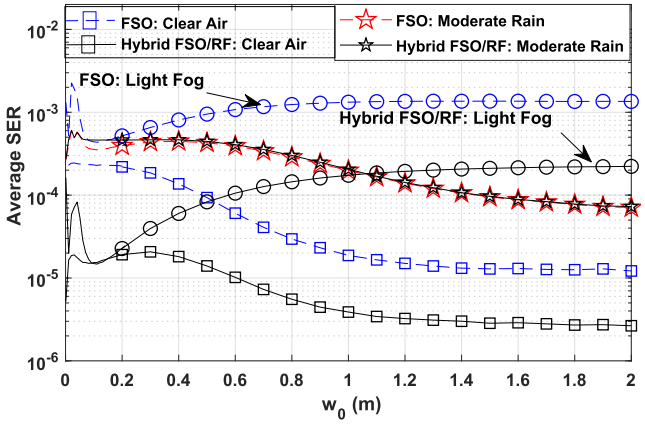

FIGURE 2. Average SER vs Beam width at the transmitter output (w_0) for different path loss attenuation.

the asymptotic regime) into (35), $B^{p}_{MRC}(\gamma_{th})$ is given by

$$B^{p^{\infty}}_{MRC}(\gamma_{th}) = \int_{\gamma_{th}}^{\infty} p(e|\gamma) f_{\gamma^{p^{\infty}}_{MRC}}(\gamma) d\gamma = B^{p^{\infty}}_{C}(\gamma_{th}) - B^{p^{\infty}}_{C,SR}(\gamma_{th}) - B^{p^{\infty}}_{SR,C}(\gamma_{th}) + B^{p^{\infty}}_{SR,SD}(\gamma_{th}) + B^{p^{\infty}}_{SD,SR}(\gamma_{th}) \quad (38)$$

The detailed derivation of each term in $B^{p}_{MRC}(\gamma_{th})$ is given in Appendix C. It is inferred from (38) that the diversity order depends on $B^{p^{\infty}}_{C}(\gamma_{th})$ or $B^{p^{\infty}}_{SR,SD}(\gamma_{th})$ or $B^{p^{\infty}}_{SD,SR}(\gamma_{th})$. Using similar arguments while calculating G_{op}, the diversity order is given by $G_{SER} = \min\{\xi^2, \beta\}$.

TABLE 3. Parameter of FSO and RF sub-systems [3], [4].

FSO/RF Parameter	Symbol	Value
Wavelength	λ_1	1.55μm
FSO Transmit Power	P^f_j	40 mW
Transmit Power	P^r_j	10 mW
Responsivity	η	0.5 $\frac{\text{A}}{\text{W}}$
Noise variance	σ^2_1	10^{-14}
jitter standard deviation	σ^j_s	30 cm
Receiver radius	a_j	10 cm
Fading severity parameter	m_j	5

Weather dependent parameters of FSO and RF channels			
Weather Condition	α_1(dB/km)	α_{rain}(dB/km)	C^2_n ($\text{m}^{-\frac{2}{3}}$)
Clear air	0.43	0	5×10^{-14}
Light Fog	20	0	3×10^{-15}
Moderate rain	5.8	5.6	5×10^{-15}

V. NUMERICAL RESULTS AND DISCUSSIONS

In the simulations, the values of FSO and RF system parameters and weather dependent parameters used in the simulations are given in Table 3. The power series based expressions in (16), (24), (25), (44) and the related equations using the power series for computing the exact outage probability and average SER values are truncated to $n = 50$, $n_1 = 10$, $n_2 = 50$, and $n_3 = 50$. We assume that R is in the middle of S and D (i.e. $L_{SR} = L_{RD} = 0.5L_{SD}$). However, the results

TABLE 4. Optimum values of beam waist at transmitter and pointing error parameter ξ_j.

a_j(cm)	L_{SD} = 500 m				
	w_0(cm)	$w_{L_{SD}}$	$w_{L_{SR}} = w_{L_{RD}}$	ξ_{SD}	$\xi_{SR} = \xi_{RD}$
5	1.5	2.61	1.77	0.47	7.82
7	**1.6**	**2.61**	**1.83**	**6.37**	**10**
10	1.8	2.64	1.98	10.3	13
15	2	2.72	2.14	14.2	15.3
a_j(cm)	L_{SD} = 1000 m				
	w_0(cm)	$w_{L_{SD}}$	$w_{L_{SR}} = w_{L_{RD}}$	ξ_{SD}	$\xi_{SR} = \xi_{RD}$
10	2.2	5.2	2.8	0.95	8.8
13	**2.5**	**5.2**	**3**	**6**	**11.2**
15	2.6	5.25	3	8.6	12.5
20	3.1	5.41	3.48	10.8	15
a_j(cm)	L_{SD} = 2000 m				
	w_0(cm)	$w_{L_{SD}}$	$w_{L_{SR}} = w_{L_{RD}}$	ξ_{SD}	$\xi_{SR} = \xi_{RD}$
20	2.5	13.4	5.23	0.88	11
27	**3**	**13.3**	**5.37**	**3.5**	**13.2**
30	4	13.4	5.89	6.4	13.7
35	5.1	13.6	6.64	8.1	13.9
a_j(cm)	L_{SD} = 3000 m				
	w_0(cm)	$w_{L_{SD}}$	$w_{L_{SR}} = w_{L_{RD}}$	ξ_{SD}	$\xi_{SR} = \xi_{RD}$
30	3.5	24.6	8.9	0.98	9.2
40	3.8	24.64	9	2.14	11.5
45	**4**	**24.66**	**9.07**	**3.5**	**13.2**
50	8	25.3	11.3	5.32	12.2

can also be plotted for any other placement of R. We consider strong turbulence conditions with $C^2_n = 1 \times 10^{-13}\text{m}^{-\frac{2}{3}}$ and the value of average SNR of RF links are assumed as $\bar{\gamma}^r_j = 5$ dB unless and otherwise stated. The values of Gamma-Gamma fading parameters α_j and β_j are calculated using (2). We assume $m_j = 5$ for which Nakagami-m distribution perfectly models fading over MMW RF channel [12], [14]–[16]. The results are plotted for independent and non-identically distributed scenarios. To satisfy the target SER of 10^{-3}, the optimal threshold SNR value for the hybrid FSO/RF system is observed to be $\gamma_{th} = 6.4$ dB using numerical optimization method suggested in [16]. Similarly, the optimal threshold SNR values for the individual FSO and RF systems to satisfy the target SER of 10^{-3} are observed to be 4.5 dB and 9 dB, respectively.

A. OPTIMUM BEAM WIDTH AND RADIUS OF RECEIVER APERTURE

Fig. 2 shows the average SER with respect to the beam waist at the transmitter output w_0 for different weather conditions given in Table 3. It can be observed that both the FSO and hybrid FSO/RF systems perform better for clear air scenario compared to other scenarios. Since the attenuation α_1 is very high for foggy environment as given in Table 3, degradation in the performance of FSO system is observed in Fig. 2. Moreover, due to the presence of the backup RF sub-system, the hybrid FSO/RF system outperforms FSO system in both clear air and foggy environment. It is also observed that the FSO link attenuation is moderate in rainy situations. Since RF link attenuation α_{rain} is high, the back-up RF sub-system does not improve the performance of FSO system as shown in Fig. 2. It is observed from the figure that the value of average SER stabilizes for w_0 greater than 80 cm. However,

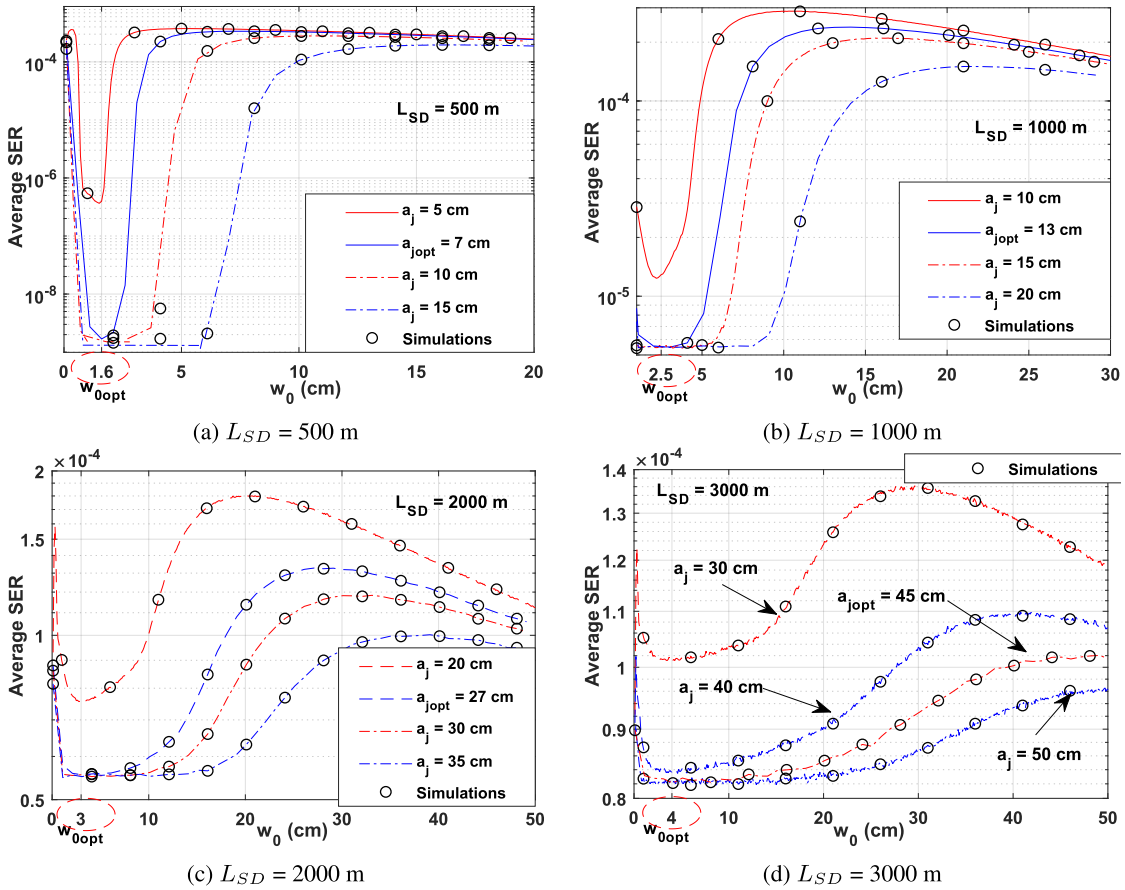

(a) $L_{SD} = 500$ m (b) $L_{SD} = 1000$ m

(c) $L_{SD} = 2000$ m (d) $L_{SD} = 3000$ m

FIGURE 3. Average SER vs beam width at the transmitter output (w_0) for different radius of receiver aperture (a_j) and link distance (L_j).

according to [30], the feasible values of w_0 and radius of receiver aperture a_j should be in terms of few centimeters for FSO transmission. It is also important to note from the figure that there is a variation in the system performance for a small value of w_0. Therefore, we need to analyze the performance of the system for small values of w_0 in terms of few centimeters, to obtain the optimum values.

To achieve the optimum beam width w_{0opt} at the transmitter output and optimum radius of receiver aperture a_{jopt}, we have plotted average SER with respect to w_0 for different values of a_j and for different link distance L_j in Fig. 3. We have tabulated the observations from Fig. 3 in Table 4. It is observed that to achieve minimum average SER value, $w_{0opt} = 1.6$ cm, 2 cm, 3 cm, and 4cm, and $a_{jopt} = 7$ cm, 13 cm, 27 cm, and 45 cm for $L_{SD} = 500$ m, 1000 m, 2000 m, and 3000 m transmission links, respectively. Table 4 shows the values of received beam waist (w_{L_j}) and ξ_j with respect to the values of w_0. The values of pointing errors parameter ξ_j, which are given in Table 4, are calculated from (8) using the values of L_j, a_j, σ_s^j and $C_n^2 = 1 \times 10^{-13}$. It is to be noted that high value of ξ_j indicates negligible pointing pointing errors and the same is observed from Fig. 3 and tabulated in Table 4. It is seen from Table 4 that to achieve minimum average SER value, $\xi_{SD_{opt}} = 6.37$, 6 , 3.5 , and 3.5 and $\xi_{SR_{opt}} = \xi_{RD_{opt}} = 10$, 11.2, 13.2, and 13.2 for $L_{SD} = 500$ m, 1000 m, 2000 m, and 3000 m transmission links, respectively. Note that any further increase in the value of ξ_j does not improve the system performance.

B. RESULTS

Fig. 4 shows the outage probability and average SER performance of the proposed system as a function of average SNR of FSO links ($\bar{\gamma}^p$) for different values of beam width at the transmitter output w_0. The corresponding values of pointing errors parameter ξ_j for a particular value of w_0 are also given in Fig. 4. The figures are plotted assuming $L_{SD} = 1000$ m, $\xi_{SR} = \xi_{RD}$, $a_j = a_{jopt} = 13$ cm, $\bar{\gamma}_j^r = 5$dB, strong turbulence conditions at $C_n^2 = 1 \times 10^{-13} \mathrm{m}^{-\frac{2}{3}}$. The simulated outage probability and average SER values closely match with the analytical values for all the SNR values as seen from the figures. This observation justifies the correctness of the proposed analysis. It is observed from Fig. 4 that for $w_0 = w_{0opt} = 2.5$ cm, both outage probability and average SER performances match the performances of no pointing errors scenario. The performance of the hybrid FSO/RF system degrades if the value of w_0 is either increased or decreased from w_{0opt}. It is also observed that the system performance degrades for a large beam waist (e.g., $w_0 = 7$ cm, 15 cm, 20 cm, and 30 cm). This is because, the beam waist at the receiver w_{L_j} is even larger compared to w_0 and the receiver

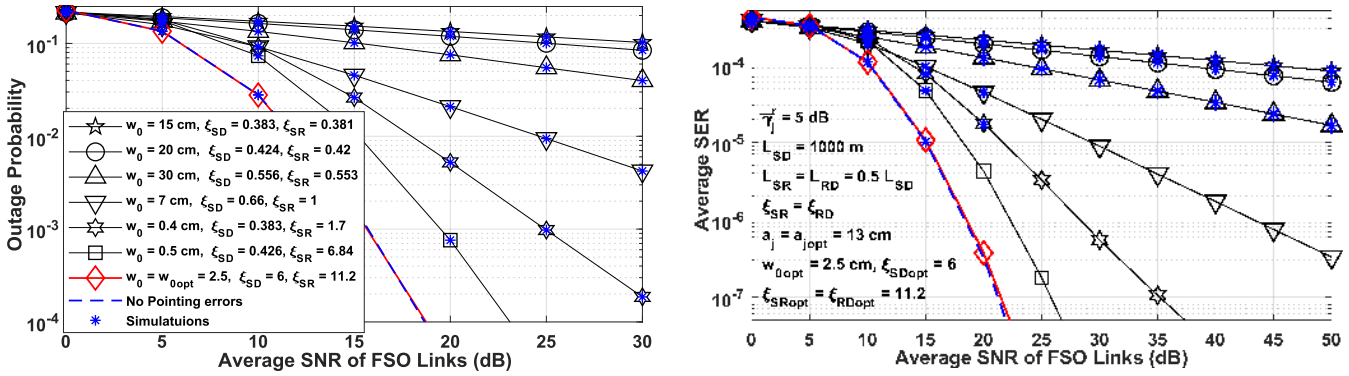

(a) Outage Probability (b) Average SER

FIGURE 4. **Outage Probability and Average SER vs average SNR of FSO links ($\bar{\gamma}^P$) of a hybrid FSO/RF system for different values of w_o and ξ_j (legends are applicable to both the graphs).**

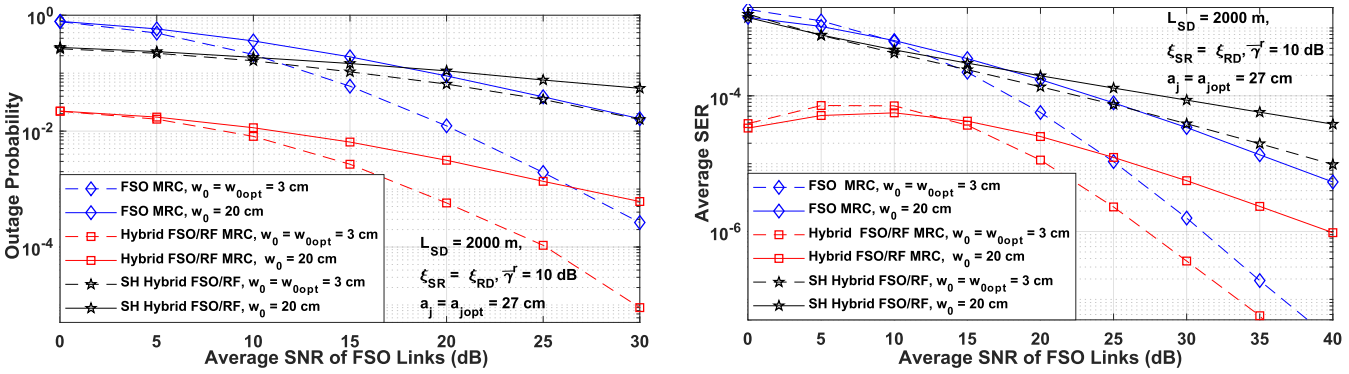

(a) Outage Probability (b) Average SER

FIGURE 5. **Outage probability and Average SER as a function of average SNR of FSO links ($\bar{\gamma}^P$) for DH FSO system with MRC, DH Hybrid FSO/RF system with MRC and SH Hybrid FSO/RF system.**

radius will be smaller to capture the beam. Therefore, when the transmitted beam size is too large, the beam size at the receiver is also large due to its geometric properties. However, if the transmitted beam size is too small (e.g., $w_0 = 0.4$ cm and 0.5 cm), then the beam size at the receiver is large due to significant diffraction of small beam. Moreover, the pointing errors severity seems tolerable for smaller beam width values compared to larger beam width values. It is noticed that to achieve SER $= 10^{-5}$ and outage probability $= 10^{-2}$, optimum beam width (i.e. $w_{0opt} = 2.5$ cm) offers the SNR gain values of more than 3 dB, 6 dB, and 15 dB compared to $w_0 = 0.5$ cm, 0.4 cm, and 7 cm, respectively. Hence, it is important to transmit with the optimum beam width in order to achieve the best performance.

Fig. 5 shows the outage probability and average SER curves with respect to the average SNR of FSO links ($\bar{\gamma}^P$) for different values of w_0 and corresponding values of ξ_j. The plots show the performances of the DH FSO system with MRC, DH hybrid FSO/RF system with MRC and SH hybrid FSO/RF system. It is observed that in order to maintain the spectral efficiency of both SH and DH hybrid FSO/RF systems equal, their corresponding switching threshold values also should be equal for fair comparison. Thus, we set the threshold values as $\gamma_{th}^{SH} = \gamma_{th}^{MRC} = 6.4$ dB and compared the performances of both the systems in Fig. 5. As mentioned above, the optimal threshold SNR value for the individual FSO system with MRC is chosen as 4.5 dB. In case of hybrid systems, the average SNR of MMW RF links is given by $\bar{\gamma}_j^r = 10$ dB. The figures are plotted for $L_{SD} = 2000$ m, $a_j = a_{jopt} = 27$ cm, and strong turbulence conditions. In addition, the performances are shown for the following two cases: (1) $w_0 = w_{0opt} = 3$ cm with the corresponding values of $\xi_{SD_{opt}} = 3.5$, $\xi_{SR_{opt}} = \xi_{RD_{opt}} = 13.2$ (i.e. insginifcant pointing errors case) and (2) $w_0 = 20$ cm and the corresponding values of $\xi_{SD} = 0.84$, $\xi_{SR} = \xi_{RD} = 0.97$ (i.e. large pointing errors case). From the plots, it is observed that the proposed cooperative DH hybrid FSO/RF system with MRC outperforms the cooperative DH FSO system with MRC for both the pointing errors scenarios due to the backup RF sub-system. In case of large pointing errors, hybrid FSO/RF system with MRC achieves an outage value of 10^{-3} and SER value of 10^{-5} with the SNR gain of more than 20 dB and 10 dB, respectively, compared to FSO system with MRC. For insignificant pointing errors, it is observed that the proposed hybrid FSO/RF with MRC achieves the outage value of 10^{-3} and SER value of 10^{-5} with the SNR gain of 8 dB and 5 dB, respectively, compared to the FSO system with MRC. By comparing the coding gains in both the

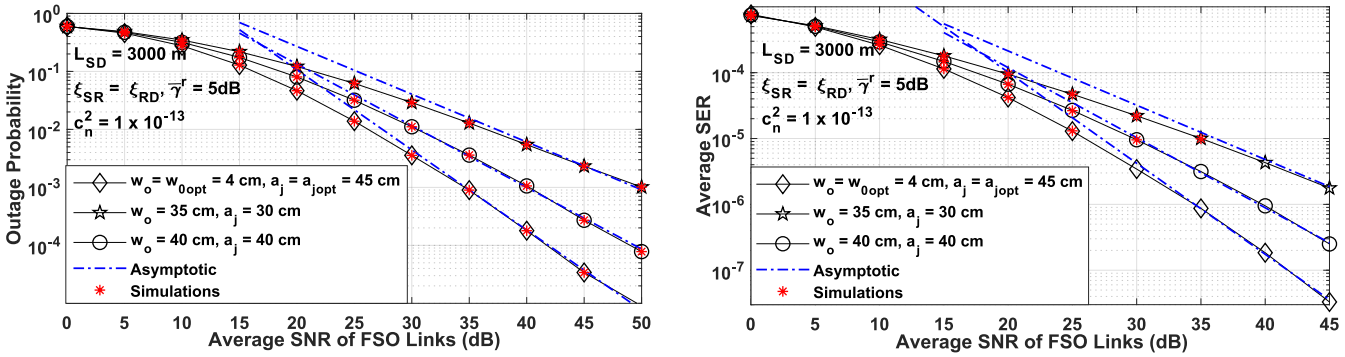

(a) Outage probability, diversity performance

(b) Average SER, diversity performance

FIGURE 6. Outage probability and Average SER vs average SNR of FSO Links ($\bar{\gamma}^p$), Analytical, asymptotic and simulated performance plots.

scenarios, it can be assessed that the backup RF sub-system is definitely improving the system performance for the case when the pointing error severity is high. It is also noticed that the hybrid FSO/RF system with MRC performs well compared to SH hybrid FSO/RF system for both the pointing errors scenarios. Moreover, this phenomenon confirms that by exploiting the diversity of DH scenario with MRC, we can achieve outage and SER performance improvement.

In Fig. 6, the diversity performance of the hybrid FSO/RF system with MRC is shown for different values of w_0 and a_j. The asymptotic outage probability and average SER performances are obtained by using (29) and (38). Table 5 shows the parameters which are used to plot the curves for three cases. The diversity order is also calculated for three cases and is given in Table 5. The derived asymptotic outage probability and average SER expressions are sufficiently tight with the exact analytical outage and SER expressions at high SNR. It is observed from the figures that large pointing error severity with small values of ξ_j adversely affect the diversity gain. However, for small pointing errors, the value of ξ_j is large enough to become less effective and the atmospheric turbulence influences the diversity gain.

TABLE 5. Diversity performance of the hybrid FSO/RF system.

$L_{SD} = 3000$ m, $C_n^2 = 1 \times 10^{-13}\text{m}^{-\frac{2}{3}}$, $\alpha_{SD} = 2.18$				
$\beta_{SD} = 1.18$, $\alpha_{SR} = \alpha_{RD} = 2.31$, and $\beta_{SR} = \beta_{RD} = 1.84$				
a_j (cm)	w_0(cm)	ξ_{SD}	$\xi_{SR} = \xi_{RD}$	$G_{op} = G_{SER}$
30	35	0.93	0.88	$\frac{\xi_{SD}^2}{2} + \frac{\xi_{SR}^2}{2} = 0.81$
40	40	1.16	1.17	$\frac{\xi_{SD}^2}{2} + \frac{\xi_{SR}^2}{2} = 1.35$
45	**4**	**3.5**	**13.2**	$\frac{\beta_{SD}}{2} + \frac{\beta_{SR}}{2}$ **= 1.51**

Fig 7 shows the variation of average SER with respect to average SNR of FSO links $\bar{\gamma}^p$ for different values of link distance L_j. We assume $\bar{\gamma}^r = 5$ dB, $w_0 = 5$ cm, $a_j = 15$ cm and $C_n^2 = 5 \times 10^{-14}$ m$^{-\frac{2}{3}}$ (i.e. moderate turbulence condition). As observed from (2) and (8), the values of α_j, β_j and ξ_j decrease with the increase in L_j, which indicates increase in the severity of atmospheric turbulence and pointing errors. This can also be observed from the figure that the system achieves an average SER value of 10^{-5} with the SNR gain of more than 4 dB with the decrease in the link distance L_{SD}.

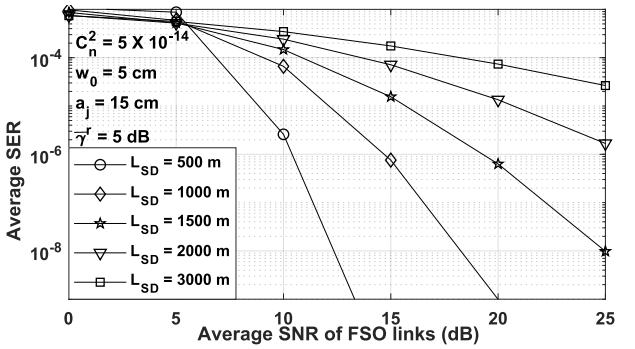

FIGURE 7. Average SER vs average SNR of FSO ($\bar{\gamma}^p$) for different values of Link distance L_j.

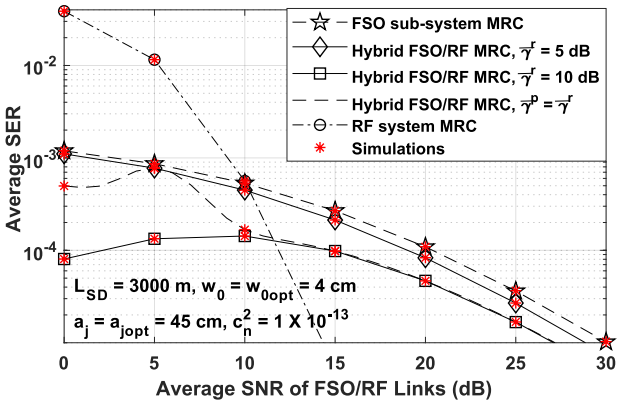

FIGURE 8. Average SER as a function of average SNR of FSO/RF links ($\bar{\gamma}^p = \bar{\gamma}^r$).

In Fig. 8, we have plotted the average SER with respect to the average SNR of FSO and RF links ($\overline{\gamma}_j^p$ and $\overline{\gamma}_j^r$), where the values of $\overline{\gamma}_j^p$ and $\overline{\gamma}_j^r$ are varied simultaneously (i.e. $\overline{\gamma}_j^p = \overline{\gamma}_j^r$). We have also plotted the average SER of the FSO and RF sub-systems with MRC as a function of $\overline{\gamma}_j^p$ and $\overline{\gamma}_j^r$, respectively. In order to compare, we have plotted the average SER of the hybrid FSO/RF system with respect to $\overline{\gamma}_j^p$ by fixing the average SNR of RF links as $\overline{\gamma}_j^r = 5$ and 10 dB. As mentioned above, the optimal threshold SNR value for the hybrid FSO/RF system is chosen as $\gamma_{th} = 6.4$ dB. Similarly, the optimal threshold SNR values for the individual

FSO and RF systems with MRC are chosen as 4.5 dB and 9 dB, respectively. In case of the hybrid FSO/RF system assuming $\overline{\gamma}_j^p = \overline{\gamma}_j^r$, it is observed that at high SNR, the average SER curves have the same slope as that of the SER curve of FSO system. This shows that at high SNR, the hybrid FSO/RF system completely depends on the FSO sub-system regardless of the SNR of the RF sub-system due to priority given to FSO transmission. Therefore, this shows that the RF sub-system does not contribute in improving the diversity gain of the overall system. However, RF sub-system helps in improving the coding gain of the system. In case of hybrid FSO/RF system with fixed value of $\overline{\gamma}_j^r$, it is observed that there is a significant improvement in the performance of the hybrid FSO/RF system with increase in the value of $\overline{\gamma}_j^r$ from 5 dB to 10 dB. It is noticed that the hybrid FSO/RF system offers the SNR gain values of 7 dB and 2 dB for $\overline{\gamma}_j^r = 10$ dB and $\overline{\gamma}_j^r = 5$ dB, respectively, to achieve the average SER value of 10^{-4} compared to the FSO sub-system. When the quality of RF link is high (i.e. $\overline{\gamma}_j^r = 10$ dB), considerable performance improvement is observed, especially in the low-SNR region. This is because at a very low value of $\overline{\gamma}_j^p$, the high-quality RF links (i.e. $\overline{\gamma}_j^r = 10$ dB) are being used frequently. Further, as the average SNR of FSO links ($\overline{\gamma}_j^p$) slightly increases, the FSO links are used more often, which are weaker than the RF links and hence, degradation in the SER performance is initially observed. When $\overline{\gamma}_j^p$ increases further, the FSO links become stronger and improvement in the SER performance is observed. It is important to note that hybrid FSO/RF system performs better than the RF system in the low SNR region, however, the RF system outperforms hybrid FSO/RF system in the high SNR region. This is due to the fact that with the increase in the transmit power of the RF system, it becomes more reliable, where as FSO system suffers from atmospheric turbulence induced fading and pointing errors. In Hybrid FSO/RF system, to achieve higher data rate, FSO sub-system transmits with higher priority and RF sub-system is used as a backup. The reason for using RF sub-system as a backup is to improve reliability in case of FSO link failure.

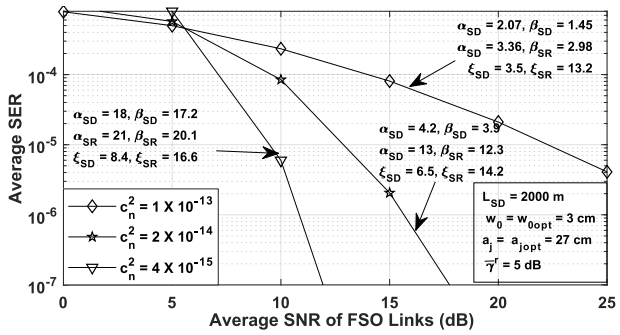

FIGURE 9. Average SER as a function of average SNR of FSO links ($\bar{\gamma}_j^p$) for different turbulence conditions.

Fig 9 shows the average SER with respect to average SNR of FSO links ($\overline{\gamma}_j^p$) for different values of atmospheric turbulence C_n^2 assuming $L_{SD} = 2000$ m, $w_0 = w_{0opt} = 3$ cm, and radius of receiver aperture $a_j = a_{jopt} = 27$ cm. The curves are plotted for $C_n^2 = 1 \times 10^{-13}$, 2×10^{-14} and 4×10^{-15} $\text{m}^{-\frac{2}{3}}$, which indicate strong, moderate and weak turbulence conditions, respectively, and the corresponding values of α_j, β_j and ξ_j are shown in the figure. The values of α_j, β_j and ξ_j are increasing with the decreasing severity of atmospheric turbulence. This can also be observed from the plots that the system achieves an average SER value of 10^{-5} with the SNR gain of 10 dB and 14 dB for moderate and weak turbulence, respectively, compared to strong turbulence.

VI. CONCLUSION

In this paper, we proposed a cooperative DF relaying-based hybrid FSO/RF system with MRC at the destination. For a realistic study of the FSO system, the effect of pointing errors in the presence of atmospheric turbulence induced fading together with path loss attenuation is considered in this paper. In order to counteract the adverse affects of the FSO links, a backup RF sub-system is used. We investigated the performance of the proposed scheme by obtaining the exact and asymptotic outage probability and average SER expressions in closed-form. It is inferred from the asymptotic expression that the diversity order of the proposed system is equal to $\min\{\xi^2, \beta\}$. The effect of pointing errors on the system performance is analyzed under different scenarios and it is observed that the pointing errors significantly degrade the diversity of the system. However, the proposed hybrid system improves the performance significantly for the case when pointing error severity is high due to backup RF sub-system. In order to validate the analytical performance parameters, an experimental measurement campaign will be carried out using a real state-of-the-art hybrid FSO/RF-based testbed as a part of our future work.

APPENDIX A
AVERAGE SER OF FSO SUB-SYSTEM

In this appendix, we define all the terms in (35) to derive the average SER of the FSO sub-system. $B_{MRC}^p(\gamma_{th})$ can be expressed as

$$B_{MRC}^p(\gamma_{th}) = \int_{\gamma_{th}}^{\infty} p(e|\gamma) f_{\gamma_{MRC}^p}(\gamma) d\gamma = B_{MRC}^p - B_{MRC}^{p_{out}}(\gamma_{th}), \tag{39}$$

where B_{MRC}^p, the average SER of FSO system, is given by

$$B_{MRC}^p = \int_0^{\infty} p(e|\gamma) f_{\gamma_{MRC}^p}(\gamma) d\gamma. \tag{40}$$

Now the average SER of FSO sub-system during the outage period (i.e. $\gamma_{MRC}^p < \gamma_{th}$) is given by

$$B_{MRC}^{p_{out}}(\gamma_{th}) = \int_0^{\gamma_{th}} p(e|\gamma) f_{\gamma_{MRC}^p}(\gamma) d\gamma. \tag{41}$$

where $p(e/\gamma)$ is the conditional SER for MPSK signaling conditioned on the instantaneous SNR of any given link γ

TABLE 6. Notations used in (45), (46), (48), (51), and (53).

$q_{1,n}^{j} = \gamma_{th}^{\Omega_{g,n}^{j}}$	$\mathcal{N}_{21,g}^{j,i,n} \triangleq \mathcal{N}_3^i, 0, \frac{1}{2}, -\Omega_{g,n}^{j}$	$\mathcal{N}_{51,RD,g}^{SD,n} \triangleq 1 - \Omega_{g,n}^{SD}, \mathcal{N}_2^{RD}$
$q_{2,n}^{j} = -\frac{2}{\sqrt{\pi}} \sum_{n_3=0}^{\infty} \mathcal{K}_{n_3} \gamma_{th}^{\Omega_{g,n}^{j}+n_3+\frac{1}{2}}$	$\mathcal{N}_{22,g}^{j,i,n} \triangleq \mathcal{N}_3^i, 0, \frac{1}{2}, -\Omega_{g,n}^{j} + n_3 + \frac{1}{2}$	$\mathcal{N}_{52,RD,g}^{SD,n} \triangleq 1 - (\Omega_{g,n}^{SD} + n_3 + \frac{1}{2}), \mathcal{N}_2^{RD}$
$\mathcal{N}_{6,g,n}^{j,i} \triangleq 1, 1 - \Omega_{g,n}^{j}, 1 - \Omega_{g,n}^{j} - \frac{1}{2}, \frac{\xi_i^2+1}{2}, \frac{\xi_i^2+2}{2}$	$\mathcal{N}_{31,RD,g}^{SD,n} \triangleq 1 - \Omega_{g,n}^{SD}, 0, \mathcal{N}_2^{RD}$	$\mathcal{N}_{61,RD,g}^{SD,n,n_1} \triangleq \mathcal{N}_{5,n_1}^{RD}, 0, -\Omega_{g,n}^{SD}$
$N_{7,g,n}^{j,i} \triangleq (\mathcal{N}_3^i, -\Omega_{g,n}^{j}, 0, \frac{1}{2})$,	$\mathcal{N}_{32,RD,g}^{SD,n} \triangleq 1 - (\Omega_{g,n}^{SD} + n_3 + \frac{1}{2}), 0, \mathcal{N}_2^{RD}$	$\mathcal{N}_{62,RD,g}^{SD,n,n_1} \triangleq \mathcal{N}_{5,n_1}^{RD}, 0, -(\Omega_{g,n}^{SD} + n_3 + \frac{1}{2})$
$\mathcal{N}_{11,g}^{j,i,n} \triangleq (1 - \Omega_{g,n}^{j}, \frac{1}{2}, \mathcal{N}_2^i)$	$\mathcal{N}_{41,RD,g}^{SD,n,n_1} \triangleq \mathcal{N}_{5,n_1}^{RD}, 1, 0, -\Omega_{g,n}^{SD}$	$\mathcal{N}_{71,g}^{j,n} \triangleq (\Omega_{g,n}^{j})$
$\mathcal{N}_{12,g}^{j,i,n} \triangleq 1 - \Omega_{g,n}^{j} + n_3 + \frac{1}{2}, \frac{1}{2}, \mathcal{N}_2^i$	$\mathcal{N}_{42,RD,g}^{SD,n,n_1} \triangleq \mathcal{N}_{5,n_1}^{RD}, 1, 0, -(\Omega_{g,n}^{SD} + n_3 + \frac{1}{2})$	$\mathcal{N}_{72,g}^{j,n} \triangleq (\Omega_{g,n}^{j} + n_3 + \frac{1}{2})$

is given by [12, Eq. 11]

$$p(e/\gamma) = \frac{A}{2}\text{erfc}\left(\sqrt{\gamma}D\right), \tag{42}$$

where $A = 1$ for modulation order $M = 2, A = 2$ for $M > 2$, $D = \sin\left(\frac{\pi}{M}\right)$ and erfc$(\cdot)$ is the complementary error function. The conditional SER can be represented in terms of Meijer G function as [20, Eq.(07.34.03.0619.01)]

$$p(e|\gamma) = \frac{A}{2\sqrt{\pi}}\text{G}_{1,2}^{2,0}\left(D^2\gamma \left| \begin{matrix} 1 \\ 0, \frac{1}{2} \end{matrix} \right.\right), \tag{43}$$

and it can also be represented using McLaurin series [25, Eq. (3.321)] as

$$p(e|\gamma) = \frac{A}{2}\left[1 - \frac{2}{\sqrt{\pi}} \sum_{n_3=0}^{\infty} \mathcal{K}_{n_3}\, \gamma^{\frac{2n_3+1}{2}}\right]. \tag{44}$$

Each term in (35) is solved using (40) and (41). $B_{j,i}^{p}(\gamma_{th})$ in (35), where $j \in \{SR, SD\}$ and $i \in \{SD, SR\}$ is solved using (39). We substitute (13), (16), and (43) in (40) and using [23, Eq. (07.34.21.0013.01)], $B_{j,i}^{p}$ is given by

$$B_{j,i}^{p} = \frac{A\pi^2\mathcal{K}_1^i\mathcal{K}_2^j}{2\sqrt{\pi}} \sum_{g=1}^{3}\sum_{n=0}^{\infty} \frac{X_{g,n}^{j}}{D^{2\Omega_{g,n}^{j}}} G_{6,9}^{6,4}\left(\frac{v_i}{D^2}|^{\frac{1}{2}}, \begin{matrix} \mathcal{N}_{6,g,n}^{j,i} \\ N_{7,g,n}^{j,i} \end{matrix}\right) \tag{45}$$

where $\mathcal{N}_{6,g,n}^{j,i}$ and $N_{7,g,n}^{j,i}$ are given in Table 6. Substituting (13), (16), and (44) into (41) and using [23, Eq. (07.34.21.0084.01)], the exact expression for $B_{j,i}^{p_{out}}(\gamma_{th})$ is given by

$$B_{j,i}^{p_{out}}(\gamma_{th}) = \frac{A\mathcal{K}_1^j\mathcal{K}_2^i\pi^2}{2} \sum_{n=0}^{\infty}\sum_{l=1}^{2}\sum_{g=1}^{3} q_{l,n}^{j} X_{g,n}^{j} \times G_{5,9}^{6,3}\left(v_i\gamma_{th} \left| \begin{matrix} \mathcal{N}_{1lg}^{j,i,n} \\ \mathcal{N}_{2lg}^{j,i,n} \end{matrix}\right.\right) \tag{46}$$

where $q_{l,n}^{j}$, $\mathcal{N}_{1l,g}^{j,i,n}$, and $\mathcal{N}_{2l,g}^{j,i,n}$ are given in Table 6. Substituting (27) and (43) in (40) and by using [23, Eq. (07.34.21.0013.01)], B_C^p is given by

$$B_C^p = \frac{A}{2\sqrt{\pi}}\mathcal{K}_1^{SD}\mathcal{K}_2^{RD}\pi^2 \sum_{n_1=0}^{\infty}\sum_{n=0}^{\infty}\sum_{g=1}^{3} \frac{1}{n_1!}\frac{X_{g,n}^{SD}}{D^{2\Omega_{g,n}^{SD}}}\text{B}\left(c, c_{n_1}^{n}\right) \times \left[\frac{1}{D^2}G_{6,9}^{6,4}\left(\frac{v_{RD}}{D^2}\left| \begin{matrix} 0, \mathcal{N}_{6,g,n}^{SD,RD} \\ \mathcal{N}_{5,n_1}^{RD}, -\Omega_{g,n}^{SD}, 1, 0 \end{matrix}\right.\right) + \Omega_{g,n}^{SD}G_{5,8}^{6,3}\left(\frac{v_{RD}}{D^2}\left| \begin{matrix} \mathcal{N}_{6,g,n}^{SD,RD} \\ \mathcal{N}_{5,n_1}^{RD}, -\Omega_{g,n}^{SD}, 0 \end{matrix}\right.\right)\right] \tag{47}$$

Substituting (27) and (44) into (41) and by using [23, Eq. (07.34.21.0084.01)], the exact expression for $B_C^{p_{out}}(\gamma_{th})$ is given by

$$B_C^{p_{out}}(\gamma_{th}) = \frac{A\mathcal{K}_1^{SD}\mathcal{K}_2^{RD}\pi^2}{2} \sum_{n_1=0}^{\infty}\sum_{n=0}^{\infty}\sum_{g=1}^{3}\sum_{l=1}^{2} \frac{q_{l,n}^{SD}X_{g,n}^{SD}\text{B}\left(c, c_{n_1}^{n}\right)}{n_1!} \times \left[\gamma_{th}G_{5,9}^{6,3}\left(\frac{v_{RD}}{\gamma_{th}^{-1}}\left| \begin{matrix} \mathcal{N}_{3l,RD,g}^{SD,n} \\ \mathcal{N}_{4l,RD,g}^{SD,n,n_1} \end{matrix}\right.\right) + \Omega_{g,n}^{SD}G_{4,8}^{6,2}\left(\frac{v_{RD}}{\gamma_{th}^{-1}}\left| \begin{matrix} \mathcal{N}_{5l,RD,g}^{SD,n} \\ \mathcal{N}_{6l,RD,g}^{SD,n,n_1} \end{matrix}\right.\right)\right] \tag{48}$$

where $\mathcal{N}_{3l,RD,g}^{SD,n}$, $\mathcal{N}_{4l,RD,g}^{SD,n,n_1}$, $\mathcal{N}_{5l,RD,g}^{SD,n}$ and $\mathcal{N}_{6l,RD,g}^{SD,n,n_1}$ are given in Table 6. The cumulative distribution function (CDF) of γ_j^p, can also be obtained by using [23, Eq.(07.34.21.0084.01)] in (12), is given by

$$F_{\gamma_j^p}(\gamma) = \mathcal{K}_2^j G_{3,7}^{6,1}\left(v_j\gamma \left| \begin{matrix} \mathcal{N}_2^j \\ \mathcal{N}_3^j, 0 \end{matrix}\right.\right), \tag{49}$$

$B_{C,SR}^{p}(\gamma_{th})$ in (35) is solved using (39). We substitute (42), (61), and (49) in (40). We use [25, Eq.(9.301)] to expand the Meijer G functions and the integral is solved using [25, Eq. (4.1.11)]. Using [31], we obtain a generalized Meijer G function of two variables and the final expression for $B_{C,SR}^{p}$ is given by (50), as shown at the top of the next page. After substituting (61), (49), and (44) into (41). We use [25, Eq.(9.301)] to expand the Meijer G functions and the integral is solved using [25, Eq.(3.191.1)]. With similar approach used in (50), the final expression for $B_{C,SR}^{p_{out}}(\gamma_{th})$ is given by

$$B_{C,SR}^{p_{out}}(\gamma_{th}) = \frac{A\mathcal{K}_1^{SD}\mathcal{K}_2^{RD}\mathcal{K}_2^{SR}\pi^2}{2} \sum_{n_1=0}^{\infty}\sum_{n=0}^{\infty}\sum_{g=1}^{3} \frac{X_{g,n}^{SD}\text{B}\left(c, c_{n_1}^{n}\right)}{n_1!} \sum_{l=1}^{2} q_{1l}^{SD}\left[\gamma_{th}G_{1,1:4,8:3,7}^{1,0:6,2:6,1}\left(\begin{matrix} \mathcal{N}_{7lg}^{SD}+1 \\ \mathcal{N}_{7lg}^{SD}+2 \end{matrix}\left| \begin{matrix} 0, \mathcal{N}_2^{RD} \\ \mathcal{N}_{5,n_1}^{RD}, 1, 0 \end{matrix}\right| \begin{matrix} \mathcal{N}_2^{SR} \\ \mathcal{N}_3^{SR}, 0 \end{matrix}\left| \begin{matrix} \frac{v_{RD}}{\gamma_{th}^{-1}}, \\ \frac{v_{SD}}{\gamma_{th}^{-1}} \end{matrix}\right.\right) + \Omega_g^{SD}G_{1,1:3,7:3,7}^{1,0:6,1:6,1}\left(\begin{matrix} \mathcal{N}_{5lg}^{SD} \\ \mathcal{N}_{7lg}^{SD}+1 \end{matrix}\left| \begin{matrix} \mathcal{N}_2^{RD} \\ \mathcal{N}_{5,n_1}^{RD}, 0 \end{matrix}\right| \begin{matrix} \mathcal{N}_2^{SR} \\ \mathcal{N}_3^{SR}, 0 \end{matrix}\left| \begin{matrix} v_{RD}\gamma_{th}, \\ v_{SD}\gamma_{th} \end{matrix}\right.\right)\right] \tag{51}$$

$$B^{p}_{C,SR} = \frac{A\mathcal{K}_1^{SD}\mathcal{K}_2^{RD}\mathcal{K}_2^{SR}\pi^2}{2\sqrt{\pi}} \sum_{n_1=0}^{\infty}\sum_{n=0}^{\infty}\sum_{g=1}^{3} \frac{1}{n_1!} X_{g,n}^{SD} \mathrm{B}\left(c, c_{n_1}^{n}\right) \times \Bigg[\frac{G_{2,1:4,8:3,7}^{2,0:6,2:6,1}\left(\begin{matrix} \Omega_{g,n}^{SD}+\frac{3}{2}, \Omega_{g,n}^{SD}+1 \\ \Omega_{g,n}^{SD}+2 \end{matrix} \middle| \begin{matrix} 0, \mathcal{N}_2^{RD} \\ \mathcal{N}_{5,n_1}^{RD}, 1, 0 \end{matrix} \middle| \begin{matrix} \mathcal{N}_2^{SR} \\ \mathcal{N}_3^{SR}, 0 \end{matrix} \middle| \frac{v_{RD}}{D^2}, \frac{v_{SR}}{D^2} \right)}{D^{2(\Omega_g^{SD}+1)}} + \frac{\Omega_g^{SD} G_{2,1:3,7:3,7}^{2,0:6,1:6,1}\left(\begin{matrix} \Omega_{g,n}^{SD}+\frac{1}{2}, \Omega_{g,n}^{SD} \\ \Omega_{g,n}^{SD}+1 \end{matrix} \middle| \begin{matrix} \mathcal{N}_2^{RD} \\ \mathcal{N}_{5,n_1}^{RD}, 0 \end{matrix} \middle| \begin{matrix} \mathcal{N}_2^{SR} \\ \mathcal{N}_3^{SR}, 0 \end{matrix} \middle| \frac{v_{RD}}{D^2}, \frac{v_{SR}}{D^2} \right)}{D^{2\Omega_g^{SD}}} \Bigg] \tag{50}$$

where $\mathcal{N}_{7l,g}^{j,n}$ is given in Table 6. $B^{p}_{SR,C}(\gamma_{th})$ in (35) is solved using (39). We substitute (16), (24) and (42) in (40). The remaining expression is solved using similar approach as in (50). The final expression for $B_{SR,C}$ is given by

$$B^{p}_{SR,C} = \frac{A\mathcal{K}_1^{SR}\pi^2}{2\sqrt{\pi}} \sum_{n=0}^{\infty}\sum_{n_1=0}^{\infty}\sum_{g=1}^{3} \frac{X_{g,n}^{SR}\mathcal{K}_{n_1}}{D^{2\Omega_g^{SR}}} G_{2,1:3,7:3,7}^{2,0:6,1:6,1} \left(\begin{matrix} \Omega_{g,n}^{SR}+\frac{1}{2}, \Omega_{g,n}^{SR} \\ \Omega_{g,n}^{SR}+1 \end{matrix} \middle| \begin{matrix} \mathcal{N}_2^{RD} \\ \mathcal{N}_{5,n_1}^{RD}, 0 \end{matrix} \middle| \begin{matrix} \mathcal{N}_{4,n_1}^{SD} \\ \mathcal{N}_3^{SD}, -(\frac{\xi_{RD}^2}{2}+n_1) \end{matrix} \middle| \frac{v_{RD}}{D^2}, \frac{v_{SD}}{D^2} \right) \tag{52}$$

Substituting (16), (24) and (44) into (41) and similar approach is used as in (51) to solve the remaining expression. The final expression for $B^{p_{out}}_{SR,C}(\gamma_{th})$ is given by

$$B^{p_{out}}_{SR,C}(\gamma_{th}) = \frac{A}{2}\mathcal{K}_1^{SR}\pi^2 \sum_{n=0}^{\infty}\sum_{n_1=0}^{\infty}\sum_{g=1}^{3}\sum_{l=1}^{2} X_{g,n}^{SR}\mathcal{K}_{n_1} q_{1l}^{SR} G_{1,1:3,7:3,7}^{1,0:6,1:6,1} \left(\begin{matrix} \mathcal{N}_{7lg}^{SR} \\ \mathcal{N}_{7lg}^{SR}+1 \end{matrix} \middle| \begin{matrix} \mathcal{N}_2^{RD} \\ \mathcal{N}_{5,n_1}^{RD}, 0 \end{matrix} \middle| \begin{matrix} \mathcal{N}_{4,n_1}^{SD} \\ \mathcal{N}_3^{SD}, -(\frac{\xi_{RD}^2}{2}+n_1) \end{matrix} \middle| \begin{matrix} v_{RD}\gamma_{th}, \\ v_{SD}\gamma_{th} \end{matrix} \right) \tag{53}$$

where $\mathcal{N}_{7l,g}^{j,n}$ is given in Table 6.

APPENDIX B
AVERAGE SER OF RF SUB-SYSTEM

In this appendix, we define all the terms in (35) to derive the average SER of the RF sub-system. In order to derive (35), we define the following functions, as given by

$$N(\lambda, \Omega, \phi, a) = \int_{\phi}^{\infty} \mathrm{erfc}(a\sqrt{Y}) Y^{\lambda-1} e^{-\Omega Y} dY = \mathrm{erfc}(a\sqrt{\phi}) \frac{\Gamma(\lambda, \Omega\phi)}{\Omega^{\lambda}} - \frac{a}{\sqrt{\pi}} \sum_{r=0}^{\lambda-1} \frac{\Omega^r}{r!} \frac{\Gamma\left(r+\frac{1}{2}, (a^2+\Omega)\phi\right)}{(a^2+\Omega)^{r+\frac{1}{2}}} \tag{54}$$

where the expression in (54) is solved using integration by parts as in [12, Eq.(18)] using [25, Eq. (2.33.10) and (2.33.11)], $\Gamma(\cdot,\cdot)$ is the upper incomplete gamma function [25, Eq. (8.350.2)] and

$$P(\lambda, \phi, a) = \int_{\phi}^{\infty} \mathrm{erfc}(a\sqrt{Y}) Y^{\lambda-1} dY = \frac{(-\phi)^{\lambda}}{\lambda} \mathrm{erfc}(a\sqrt{\phi}) + \frac{a^{-2\lambda}}{\lambda\sqrt{\pi}} \Gamma\left(\lambda+\frac{1}{2}, a^2\phi\right) \tag{55}$$

The integral in (55) is solved using MATHEMATICA. To solve $B^{r}_{j,i}(\gamma^{r}_{th})$, where $j \in \{SD, SR\}$ and $i \in \{SR, SD\}$, we substitute (19), (20), and (42) in (35). Using [25, Eq.(8.352.6)] and (54), $B^{r}_{j,i}(\gamma^{r}_{th})$ is given by

$$B^{r}_{j,i}(\gamma^{r}_{th}) = \frac{A w_j^{m_j}}{2\Gamma(m_j)} \Bigg[N\left(m_j, w_j, \gamma^{r}_{th}, D\right) - \sum_{k_2=0}^{m_i-1} \frac{w_i^{k_2}}{k_2!} N\left(m_j+k_2, w_{j,i}, \gamma^{r}_{th}, D\right) \Bigg] \tag{56}$$

where $w_{j,i} \triangleq w_j + w_i$. To solve $B^{r}_{C}(\gamma^{r}_{th})$, we substitute (26) and (42) in (35). Using (54) and (55), $B^{r}_{C}(\gamma^{r}_{th})$ is given by

$$B^{r}_{C}(\gamma^{r}_{th}) = \frac{A}{2} \sum_{n_2=0}^{\infty} \sum_{k_1=0}^{m_{RD}+n_2} C_{n_2}^{k_1} (C_{k_1}^{m} - 1)! \Bigg[P(C_{n_2,k_1}^{m}, \gamma^{r}_{th}, D) \times C_{n_2,k_1}^{m} - \sum_{p_1=0}^{C_{k_1}^{m}-1} \frac{w_{SD}^{p_1}}{p_1!} C_{n_2,k_1}^{m,p_1} N(C_{n_2,k_1}^{m,p_1}, w_{SD}, \gamma^{r}_{th}, D) + \sum_{p_1=0}^{C_{k_1}^{m}-1} \frac{w_{SD}^{p_1+1}}{p_1!} N(C_{n_2,k_1}^{m,p_1}+1, w_{SD}, \gamma^{r}_{th}, D) \Bigg], \tag{57}$$

To solve $B^{r}_{C,SR}(\gamma^{r}_{th})$, we substitute (26) and (20) in (35). Using [29, Eq.(8.352.6)], (54) and (55), $B^{r}_{C,SR}(\gamma^{r}_{th})$ is given by (58), as shown at the bottom of the next page.

To solve $B^{r}_{SR,C}(\gamma^{r}_{th})$, we substitute (25) and (19) in (35). Using [29, Eq.(8.352.6)], (54) and (55), $B^{r}_{SR,C}(\gamma^{r}_{th})$ is given by (59), as shown at the bottom of the next page.

APPENDIX C
ASYMPTOTIC SER ANALYSIS OF FSO SUB-SYSTEM

In this appendix, we define the terms in (38) to derive the asymptotic average SER of the hybrid system. By applying [23, Eq. (07.34.06.0040.01)] in (12) and (13), the resultant expression along with (43) are substituted into (38). The remaining integral is solved using [23, Eq. (07.34.21.0085.01)]. Finally, the closed-form expression of $B_{j,i}^{\infty p}(\gamma_{th})$, where $j \in \{SR, SD\}$ and $i \in \{SD, SR\}$, is given by

$$B_{j,i}^{\infty p}(\gamma_{th}) = \sum_{k=1}^{3}\sum_{k_3=1}^{3} \frac{A\mathcal{K}_1^j \mathcal{K}_1^i \Lambda_{x_{1,k_3,k}} \Lambda_{4,k_3}^j \Lambda_{1,k}^i}{2\sqrt{\pi}} \times \left(\bar{\gamma}_j^p\right)^{-v_j} \left(\bar{\gamma}_i^p\right)^{-v_i}, \quad (60)$$

where $\Lambda_{x_{1,k_3,k}}$ and $x_{1,k_3,k}$ are given in Table 7. In order to obtain simple expressions for $B_C^{\infty p}(\gamma_{th})$ and $B_{C,SR}^{\infty p}(\gamma_{th})$, we recalculate $f_{\gamma_C^p}(\gamma)$ by differentiating (24) with respect to γ to obtain

$$f_{\gamma_C^p}(\gamma) = \sum_{n_1=0}^{\infty} \mathcal{K}_{n_1} \gamma^{-1} \left[G_{4,8}^{6,2}\left(v_{RD}\gamma \middle| \begin{matrix} 0, \mathcal{N}_2^{RD} \\ \mathcal{N}_{5,n_1}^{RD}, 1, 0 \end{matrix}\right) \times G_{3,7}^{6,1}\left(v_{SD}\gamma \middle| \begin{matrix} \mathcal{N}_4^{SD} \\ \mathcal{N}_3^{SD}, -(\frac{\xi_{SD}^2}{2}+n_1) \end{matrix}\right) + G_{3,7}^{6,1}\left(v_{RD}\gamma \middle| \begin{matrix} \mathcal{N}_2^{RD} \\ \mathcal{N}_{5,n_1}^{RD}, 0 \end{matrix}\right) \times G_{4,8}^{6,2}\left(v_{SD}\gamma \middle| \begin{matrix} 0, \mathcal{N}_4^{SD} \\ \mathcal{N}_{5,n_1}^{SD}, -(\frac{\xi_{SD}^2}{2}+n_1), 1 \end{matrix}\right)\right] \quad (61)$$

The procedure to solve $B_C^{\infty p}(\gamma_{th})$ is similar to that of solving (60). Finally, the closed-form expression of $B_C^{\infty p}(\gamma_{th})$ is given by

$$B_C^{\infty p}(\gamma_{th}) = \sum_{n_1=0}^{\infty}\sum_{k=1}^{6} \frac{A\mathcal{K}_{n_1} \Lambda_{x_{2,n_1,k}}}{2\sqrt{\pi}} \left[\Lambda_{2,k}^{RD,n_1} \Lambda_{6,k}^{SD,n_1} + \Lambda_{3,k}^{SD,n_1} \Lambda_{5,k}^{RD,n_1}\right] \left[\bar{\gamma}_{SD}^p\right]^{-v_{SD}} \left[\bar{\gamma}_{RD}^p\right]^{-v_{RD}}, \quad (62)$$

TABLE 7. Notations used in asymptotic SER analysis.

$\Lambda_{4,k_3}^j = \sum_{k_3=1}^{3} \frac{\prod_{q=1,q\neq k_3}^{3} \Gamma(\mathcal{N}_{1,q}^j - N_{1,k_3}^j)}{\Gamma(1+\xi^2-N_{1,k_3}^j)} \left(\alpha_j\beta_j\kappa_j\right)^{N_{1,k_3}^j}$
$\Lambda_{5,k}^{j,n_1} \triangleq \frac{\prod_{q=1,q\neq k}^{6} \Gamma(\mathcal{N}_{5,n_1 q}^j - N_{5,n_1 k}^j)}{\prod_{q=2}^{3} \Gamma(\mathcal{N}_{2,q}^j - N_{5,n_1,k}^j)} \left[\frac{(\alpha_j\beta_j\kappa_j)^2}{16}\right]^{N_{5,k}^j}$
$\Lambda_{6,k}^{j,n_1} \triangleq \left(\Lambda_{3,k}^{j,n_1} \frac{\Gamma(1+\mathcal{N}_{3,k}^j)}{\Gamma(\mathcal{N}_{3,k}^j)}\right), \Lambda_{x_g} \triangleq (\gamma_{th})^{x_g}\, G_{2,3}^{3,0}\left(D^2\gamma_{th} \middle| \begin{matrix} 1, 1-x_g \\ -x_g, 0, \frac{1}{2} \end{matrix}\right)$
$x_{1,k_3,k} \triangleq \left(\frac{N_{1,k}^j}{2} + \frac{N_{1,k_3}^i}{2}\right), x_{2,n_1,k} \triangleq \left(\mathcal{N}_{3,k}^{SD} + \mathcal{N}_{5,n_1,k}^{RD}\right)$
$x_{3,n_1,k} \triangleq \left(\mathcal{N}_{1,k}^{SR} + \mathcal{N}_{3,k}^{SD} + \mathcal{N}_{5,n_1,k}^{RD}\right)$
$x_{4,n_1,k,k_3} \triangleq \left(\mathcal{N}_{5,n_1,k}^{RD} + \mathcal{N}_{3,k}^{SD} + N_{1,k_3}^{SR}\right)$

where $\Lambda_{5,k}^{j,n_1}$, $\Lambda_{6,k}^{j,n_1}$, $\Lambda_{x_{2,n_1,k}}$, and $x_{2,n_1,k}$ are given in Table 7. Using a similar approach as in (60), a closed-form expression of $B_{C,SR}^{\infty p}(\gamma_{th})$ is given by

$$B_{C,SR}^{\infty p}(\gamma_{th}) = \sum_{n_1=0}^{\infty}\sum_{k=1}^{6} \frac{A\mathcal{K}_{n_1} \mathcal{K}_1^{SR} \Lambda_{x_{3,n_1,k}} \Lambda_{1,k}^{SR}}{2\sqrt{\pi}} \left[\Lambda_{2,k}^{RD,n_1} \Lambda_{6,k}^{SD,n_1} + \Lambda_{3,k}^{SD,n_1} \Lambda_{5,k}^{RD,n_1}\right] \left[\bar{\gamma}_{SR}^p\right]^{-v_{SR}} \left[\bar{\gamma}_{RD}^p\right]^{-v_{RD}} \left[\bar{\gamma}_{SD}^p\right]^{-v_{SD}}, \quad (63)$$

where $\Lambda_{x_{3,n_1,k}}$ and $x_{3,n_1,k}$ are given in Table 7. The closed-form expression for $B_{SR,C}^{\infty p}(\gamma_{th})$ can be obtained with a similar approach used in (60) and the expression is given by

$$B_{SR,C}^{\infty p}(\gamma_{th}) = \sum_{n_1=0}^{\infty}\sum_{k=1}^{6}\sum_{k_3=1}^{3} \frac{A\mathcal{K}_{n_1} \mathcal{K}_1^{SR} \Lambda_{4,k_3}^{SR} \Lambda_{3,k}^{RD,n_1} \Lambda_{2,k}^{SD,n_1}}{2\sqrt{\pi}} \times \Lambda_{x_{4,n_1,k,k_3}} \times \left[\bar{\gamma}_{SR}^p\right]^{-v_{SR}} \left[\bar{\gamma}_{RD}^p\right]^{-v_{RD}} \left[\bar{\gamma}_{SD}^p\right]^{-v_{SD}}, \quad (64)$$

$\Lambda_{x_{4,n_1,k,k_3}}$ and x_{4,n_1,k,k_3} are given in Table 7.

$$B_{C,SR}^{r}(\gamma_{th}^r) = \frac{A}{2}\sum_{n_2=0}^{\infty}\sum_{k_1=0}^{m_{RD}+n_2} C_{n_2}^{k_1} (C_{k_1}^m - 1)! \Bigg[C_{n_2,k_1}^m \left\{ P(C_{n_2,k_1}^m, \gamma_{th}^r, D) - \sum_{k_2=0}^{m_{SR}-1} \frac{w_{SR}^{k_2}}{k_2!} N(C_{n_2,k_1}^m + k_2 + 1, w_{SD}, \gamma_{th}^r, D)\right\} - \sum_{p_1=0}^{C_{k_1}^m - 1} \frac{w_{SD}^{p_1}}{p_1!}(C_{n_2,k_1}^m + p_1)\left\{ N(C_{n_2,k_1}^{m,p_1}, w_{SD}, \gamma_{th}^r, D) - \sum_{k_2=0}^{m_{SR}-1} \frac{w_{SR}^{k_2}}{k_2!} N(C_{n_2,k_1}^{m,p_1} + k_2, w_{SD,SR}, \gamma_{th}^r, D)\right\} + \sum_{p_1=0}^{C_{k_1}^m - 1} \frac{w_{SD}^{p_1+1}}{p_1!}\left\{ N(C_{n_2,k_1}^{m,p_1} + 1, w_{SD}, \gamma_{th}^r, D) - \sum_{k_2=0}^{m_{SR}-1} \frac{w_{SR}^{k_2}}{k_2!} N(C_{n_2,k_1}^{m,p_1} + k_2 + 1, w_{SD,SR}, \gamma_{th}^r, D)\right\}\Bigg] \quad (58)$$

$$B_{SR,C}^{r}(\gamma_{th}^r) = \frac{A}{2}\sum_{n_2=0}^{\infty}\sum_{k_1=0}^{m_{RD}+n_2} C_{n_2}^{k_1} \frac{w_{SR}^{m_{SR}}}{\Gamma(m_{SR})} (C_{k_1}^m - 1)! N(C_{n_2,k_1}^m + m_{SR}, w_{SR}, \gamma_{th}^r, D) - \sum_{k_2=0}^{m_{SD}-1} \frac{w_{SD}^{k_2}}{k_2!} N(C_{n_2,k_1}^m + m_{SR} + k_2, w_{SD,SR}, \gamma_{th}^r, D) \quad (59)$$

ACKNOWLEDGMENT

The authors would like to thank the anonymous reviewers and the editor for their constructive comments and suggestions which helped us to improve the quality of the paper.

REFERENCES

[1] M. A. Khalighi and M. Uysal, "Survey on free space optical communication: A communication theory perspective," *IEEE Commun. Surveys Tuts.*, vol. 16, no. 4, pp. 2231–2258, 4th Quart., 2014.

[2] B. He and R. Schober, "Bit-interleaved coded modulation for hybrid RF/FSO systems," *IEEE Trans. Commun.*, vol. 57, no. 12, pp. 3753–3763, Dec. 2009.

[3] E. Lee, J. Park, D. Han, and G. Yoon, "Performance analysis of the asymmetric dual-hop relay transmission with mixed RF/FSO links," *IEEE Photon. Technol. Lett.*, vol. 23, no. 21, pp. 1642–1644, Nov. 1, 2011.

[4] H. Samimi and M. Uysal, "End-to-end performance of mixed RF/FSO transmission systems," *IEEE/OSA J. Opt. Commun. Netw.*, vol. 5, no. 11, pp. 1139–1144, Nov. 2013.

[5] E. Balti and M. Guizani, "Mixed RF/FSO cooperative relaying systems with co-channel interference," *IEEE Trans. Commun.*, vol. 66, no. 9, pp. 4014–4027, Sep. 2018.

[6] S. Anees and M. R. Bhatnagar, "Performance evaluation of decode-and-forward dual-hop asymmetric radio frequency-free space optical communication system," *IET Optoelectron.*, vol. 9, no. 5, pp. 232–240, Oct. 2015.

[7] S. Anees and M. R. Bhatnagar, "Performance of an amplify-and-forward dual-hop asymmetric RF–FSO communication system," *IEEE/OSA J. Opt. Commun. Netw.*, vol. 7, no. 2, pp. 124–135, Feb. 2015.

[8] G. T. Djordjevic, M. I. Petkovic, A. M. Cvetkovic, and G. K. Karagiannidis, "Mixed RF/FSO relaying with outdated channel state information," *IEEE J. Sel. Areas Commun.*, vol. 33, no. 9, pp. 1935–1948, Sep. 2015.

[9] K. Kumar and D. K. Borah, "Quantize and encode relaying through FSO and hybrid FSO/RF links," *IEEE Trans. Veh. Technol.*, vol. 64, no. 6, pp. 2361–2374, Jun. 2015.

[10] S. Anees, P. Meerur, and M. R. Bhatnagar, "Performance analysis of a DF based dual hop mixed RF-FSO system with a direct RF link," in *Proc. IEEE GlobalSIP*, Dec. 2015, pp. 1332–1336.

[11] N. D. Chatzidiamantis, G. K. Karagiannidis, E. E. Kriezis, and M. Matthaiou, "Diversity combining in hybrid RF/FSO systems with PSK modulation," in *Proc. IEEE ICC*, Jun. 2011, pp. 1–6.

[12] M. Usman, H.-C. Yang, and M.-S. Alouini, "Practical switching-based hybrid FSO/RF transmission and its performance analysis," *IEEE Photon. J.*, vol. 6, no. 5, Oct. 2014, Art. no. 7902713.

[13] A. Touati, A. Abdaoui, F. Touati, M. Uysal, and A. Bouallegue, "On the effects of combined atmospheric fading and misalignment on the hybrid FSO/RF transmission," *J. Opt. Commun. Netw.*, vol. 8, no. 10, pp. 715–725, Oct. 2016.

[14] T. Rakia, H.-C. Yang, M.-S. Alouini, and F. Gebali, "Outage analysis of practical FSO/RF hybrid system with adaptive combining," *IEEE Commun. Lett.*, vol. 19, no. 8, pp. 1366–1369, Aug. 2015.

[15] S. Sharma, A. S. Madhukumar, and R. Swaminathan, "Switching-based hybrid FSO/RF transmission for DF relaying system," in *Proc. IEEE WCNC*, Apr. 2018, pp. 1–6.

[16] S. Sharma, A. S. Madhukumar, and R. Swaminathan, "Switching-based cooperative decode-and-forward relaying for hybrid FSO/RF networks," *IEEE/OSA J. Opt. Commun. Netw*, vol. 11, no. 6, pp. 267–281, Jun. 2019.

[17] W. Gappmair, "Further results on the capacity of free-space optical channels in turbulent atmosphere," *IET Commun.*, vol. 5, no. 9, pp. 1262–1267, Jun. 2011.

[18] M. Uysal, J. Li, and M. Yu, "Error rate performance analysis of coded free-space optical links over gamma-gamma atmospheric turbulence channels," *IEEE Trans. Wireless Commun.*, vol. 5, no. 6, pp. 1229–1233, Jun. 2006.

[19] M. R. Bhatnagar and Z. Ghassemlooy, "Performance analysis of gamma–gamma fading FSO MIMO links with pointing errors," *J. Lightw. Technol.*, vol. 34, no. 9, pp. 2158–2169, May 1, 2016.

[20] E. Bayaki, R. Schober, and R. K. Mallik, "Performance analysis of MIMO free-space optical systems in gamma-gamma fading," *IEEE Trans. Commun.*, vol. 57, no. 11, pp. 3415–3424, Nov. 2009.

[21] J. N. Laneman, D. N. C. Tse, and G. W. Wornell, "Cooperative diversity in wireless networks: Efficient protocols and outage behavior," *IEEE Trans. Inf. Theory*, vol. 50, no. 12, pp. 3062–3080, Dec. 2004.

[22] A. A. Farid and S. Hranilovic, "Outage capacity optimization for free-space optical links with pointing errors," *J. Lightw. Technol.*, vol. 25, no. 7, pp. 1702–1710, Jul. 2007.

[23] *Mathematica Edition: Version 8.0*, Wolfram Res., Champaign, IL, USA, 2010.

[24] K. Roach, "Meijer-G function representations," in *Proc. ACM Int. Conf. Symbolic Algebr. Comput.*, Jul. 1997, pp. 205–211.

[25] I. S. Gradshteyn and I. M. Ryzhik, *Table of Integrals, Series, and Products*, 7th ed. San Diego, CA, USA: Academic, 2007.

[26] M. R. Bhatnagar, "A one bit feedback based beamforming scheme for FSO MISO system over gamma-gamma fading," *IEEE Trans. Commun.*, vol. 63, no. 4, pp. 1306–1318, Apr. 2015.

[27] A. Prudnikov, Y. Brychkov, and O. Marichev, *Integrals and Series*, vol. 3. Boca Raton, FL, USA: CRC Press, 1999.

[28] G. K. Karagiannidis, N. C. Sagias, and T. A. Tsiftsis, "Closed-form statistics for the sum of squared Nakagami-m variates and its applications," *IEEE Trans. Commun.*, vol. 54, no. 8, pp. 1353–1359, Aug. 2006.

[29] E. W. Ng and M. Geller, "A table of integrals of the error functions," *J. Res. Nat. Bur. Standards*, vol. 73, no. 1, pp. 1–20, 1969.

[30] A. E. Willner, G. Xie, L. Li, Y. Ren, Y. Yan, N. Ahmed, Z. Zhao, Z. Wang, C. Liu, A. J. Willner, N. Ashrafi, S. Ashrafi, M. Tur, and A. F. Molisch, "Design challenges and guidelines for free-space optical communication links using orbital-angular-momentum multiplexing of multiple beams," *J. Opt.*, vol. 18, no. 7, 2016, Art. no. 074014.

[31] B. L. Sharma and R. F. A. Abiodun, "Generating function for generalized function of two variables," *Proc. Amer. Math. Soc.*, vol. 46, no. 1, pp. 69–72, Oct. 1974.

[32] A. Jurado-Navas, J. M. Garrido-Balsells, J. F. Paris, and A. Puerta-Notario, "A unifying statistical model for atmospheric optical scintillation," in *Numerical Simulations of Physical and Engineering Processes*. Rijeka, Croatia: InTech, Sep. 2011, pp. 181–206.

[33] M. A. Kashani, M. Uysal, and M. Kavehrad, "A novel statistical channel model for turbulence-induced fading in free-space optical systems," *J. Lightw. Technol.*, vol. 33, no. 11, pp. 2303–2312, Jun. 1, 2015.

SHUBHA SHARMA received the B.Tech. degree in electronics and communication engineering from UPTU, India, and the M.Tech. degree in communication systems from IIIT Delhi, India. She is currently pursuing the Ph.D. degree with the School of Computer Science and Engineering, Nanyang Technological University (NTU), Singapore. Her current research interests include the hybrid free-space optics/radio frequency communication systems for the back-haul networks, next-generation terrestrial communication and satellite communications, performance analysis of wireless communication systems over fading channels, and cooperative communications.

A. S. MADHUKUMAR received the B.Tech. degree from the College of Engineering, Trivandrum, India, the M.Tech. degree from the Cochin University of Science and Technology, India, and the Ph.D. degree from the Department of Computer Science and Engineering, IIT Madras, India.

He was involved in communications and signal processing research at the Centre for Development of Advanced Computing (Electronics Research and Development Centre), Government of India, and the Centre for Wireless Communications, Institute for Infocomm Research, Singapore. He is currently an Associate Professor with the School of Computer Engineering, Nanyang Technological University, Singapore. He has published over 275 refereed international conference and journal articles. His research interests include multi-tier cellular architecture, cooperative and cognitive radio systems, interference management, coding and modulation, new multiple access schemes, hybrid radio systems, and other advanced signal processing algorithms for future communication systems. He was a recipient of the Nanyang Award for Teaching Excellence, in 2007, and the Best Paper Awards at the IEEE 35th Digital Avionics Conference, in 2016, and the IEEE Integrated Communications, Navigations and Surveillance Conference, in 2016 and 2017. He is involved in a number of funded research projects, organizing international conferences, and a permanent Reviewer for many internationally reputed journals and conferences.

R. SWAMINATHAN received the B.Tech. degree in ECE from SASTRA University, Thanjavur, in 2009, the M.E. degree in communication systems from the College of Engineering Guindy, Anna University, Chennai, in 2011, and the Ph.D. degree from IIT Kharagpur, in 2016. He was a Postdoctoral Research Fellow with Nanyang Technological University (NTU), Singapore, from 2016 to 2019. He joined IIT Indore as an Assistant Professor. His current research interests include designing hybrid free-space optics/radio frequency communication systems for next-generation terrestrial and satellite communication, proposing algorithms for blind parameter estimation of forward error correcting codes and interleavers considering non-cooperative scenarios, and validating the same using real data obtained from hardware testbed. In addition, his research interests include but not limited to power line communication, index modulation techniques for next-generation wireless communication, simultaneous lightwave information and power transfer (SLIPT), nonorthogonal multiple access (NOMA) techniques, and automatic channel code and interleaver identification techniques. He received the Gold Medal from the College of Engineering Guindy, Anna University. He has been serving as a Reviewer for reputed IEEE journals and as a TPC Member of reputed IEEE conferences.